

# Constraints on anomalous quartic gauge couplings via $W\gamma jj$ production at the LHC\*

Yu-Chen Guo(郭禹辰)<sup>1)</sup> Ying-Ying Wang(王莹莹) Ji-Chong Yang(杨冀翀)<sup>2)</sup> Chong-Xing Yue(岳崇兴)<sup>3)</sup>

Department of Physics, Liaoning Normal University, Dalian 116029, China

**Abstract:** Vector boson scattering at the Large Hadron Collider (LHC) is sensitive to anomalous quartic gauge couplings (aQGCs). In this study, we investigate the aQGC contribution to  $W\gamma jj$  production at the LHC with  $\sqrt{s} = 13$  TeV in the context of an effective field theory (EFT). The unitarity bound is applied as a cut on the energy scale of this production process, which is found to have significant suppressive effects on signals. To enhance the statistical significance, we analyze the kinematic and polarization features of the aQGC signals in detail. We find that the polarization effects induced by aQGCs are unique and can discriminate the signals from the SM backgrounds well. With the proposed event selection strategy, we obtain the constraints on the coefficients of dimension-8 operators with current luminosity. The results indicate that the process  $pp \rightarrow W\gamma jj$  is powerful for searching for the  $O_{M_{2,3,4,5}}$  and  $O_{T_{5,6,7}}$  operators.

**Keywords:** anomalous quartic gauge coupling, vector boson scattering, Large Hadron Collider, Standard Model effective field theory

**DOI:** 10.1088/1674-1137/abb4d2

## 1 Introduction

Over the past few decades, most of the experimental measurements have been in good agreement with the predictions of the Standard Model (SM). The search for new physics beyond the SM (BSM) is one of the main objectives of current and future colliders. Among the processes measured at the Large Hadron Collider (LHC), vector boson scattering (VBS) processes provide ideal conditions to study BSM. It is well known that the perturbative unitarity of the longitudinal  $W_L Z_L \rightarrow W_L Z_L$  scattering is violated without the Higgs boson, which sets an upper bound on the mass of the Higgs boson [1]. In other words, with the discovery of the Higgs boson, the Feynman diagrams of the VBS processes cancel each other and the cross sections do not grow with centre-of-mass (c.m.) energy. However, such suppression of the cross section can be relaxed in the presence of new physics particles. Consequently, the cross section may be significantly in-

creased and a window to detect BSM is open [2, 3].

A model-independent approach, called the SM effective field theory (SMEFT) [4-6], has been used widely to search for BSM. In the SMEFT, the SM is a low energy effective theory of some unknown BSM theory. When the c.m. energy is not sufficient to produce the new resonance states directly and when the new physics sector is decoupled, one can integrate out the new physics particles. Then, the BSM effects become new interactions of known particles. Formally, the new interactions appear as higher dimensional operators. The VBS processes are suitable for investigating the existence of new interactions involving electroweak symmetry breaking (EWSB), which is contemplated in many BSM scenarios. The operators w.r.t. EWSB up to dimension-8 can contribute to the anomalous trilinear gauge couplings (aTGCs) and anomalous quartic gauge couplings (aQGCs). There are many full models that contain these operators, for example, anomalous gauge-Higgs couplings, composite Higgs, warped extra dimensions, 2HDM,  $U(1)_{L_\mu-L_\tau}$ , as

Received 26 May 2020, Revised 2 August 2020, Published online 18 September 2020

\* Supported in part by the National Natural Science Foundation of China (11905093, 11875157, 11947402) and the Doctoral Start-up Foundation of Liaoning Province (2019-BS-154)

1) E-mail: ycguo@lnnu.edu.cn

2) E-mail: yangjichong@lnnu.edu.cn

3) E-mail: cxyue@lnnu.edu.cn



Content from this work may be used under the terms of the Creative Commons Attribution 3.0 licence. Any further distribution of this work must maintain attribution to the author(s) and the title of the work, journal citation and DOI. Article funded by SCOAP<sup>3</sup> and published under licence by Chinese Physical Society and the Institute of High Energy Physics of the Chinese Academy of Sciences and the Institute of Modern Physics of the Chinese Academy of Sciences and IOP Publishing Ltd

well as axion-like particle scenarios [7-18].

Both aTGCs and aQGCs could impact VBS processes [19-22]. Unlike aTGCs, which also affect the diboson productions and the vector boson fusion (VBF) processes [2, 3, 23, 24], the most sensitive processes for aQGCs are the VBS processes. The dimension-8 operators can contribute to aTGCs and aQGCs independently. Therefore, we focus on the dimension-8 anomalous quartic gauge-boson operators. Moreover, it is possible that higher dimensional operators contributing to aQGCs exist without dimension-6 operators. This situation arises in the Born-Infeld (BI) theory proposed in 1934 [25], which is a nonlinear extension of the Maxwell theory motivated by a "unitarian" standpoint. It could provide an upper limit on the strength of the electromagnetic field. In 1985, the BI theory was reborn in models inspired by M-theory [26, 27]. We note that the constraint on the BI extension of the SM has recently been presented via dimension-8 operators in the SMEFT [28].

Historically, VBS has been proposed as a means to test the structure of EWSB since the early stage of planning for the Superconducting Super Collider (SSC) [29]. The study of VBS has attracted significant attention during the past few years. The first report of constraints on dimension-8 aQGCs at the LHC is from the same-sign  $WW$  production [30, 31]. At present, a number of experimental results in VBS have been obtained, including the electroweak-induced production of  $Z\gamma jj$ ,  $W\gamma jj$  at  $\sqrt{s} = 8$  TeV and  $ZZjj$ ,  $WZjj$ ,  $W^+W^+jj$  at  $\sqrt{s} = 13$  TeV [32-39]. Furthermore, theoretical studies have been extensively performed [40-44]. Among these VBS processes, in this paper we consider  $W\gamma jj$  production via scattering between  $Z/\gamma$  and  $W$  bosons. The next-to-leading order (NLO) QCD corrections to the process  $pp \rightarrow W\gamma jj$  have been computed in Refs. [21, 45], and the  $K$  factor has been found to be close to 1 ( $K \approx 0.97$  [21]). However, the phenomenology of this process with aQGCs needs further investigation.

The SMEFT is valid only under a certain energy scale  $\Lambda$ . The validity of the SMEFT with dimension-8 operators is an important issue that has been ignored in previous experiments. The amplitude of VBS with aQGCs increases as  $O(E^4)$ , leading to tree-level unitarity violation at high enough energies [46-48]. In such a case, it is inappropriate to use the SMEFT. A unitarity bound should be set to prevent the violation of unitarity. The unitarity bound is often regarded as a constraint on the coefficient of a high dimensional operator. However, this constraint is not feasible in VBS processes because the energy scale of the sub-process is not a fixed value but a distribution. To consider validity, it is proposed that [49] the constraints obtained by experiments should be reported as functions of energy scales. However, in the  $W\gamma jj$  production, the energy scale of sub-process  $\hat{s} = (p_W + p_\gamma)^2$  is not an observable. In this study, we obtain an approximation

of  $\hat{s}$ , based on which the unitarity bounds are applied as limits on the events at fixed coefficients. The unitarity bounds will suppress the number of signal events.

To enhance the discovery potentiality of the signal, we have to optimize the event selection strategy. With the approximation of  $\hat{s}$ , other limits to cut off the small  $\hat{s}$  events become redundant. Therefore, we investigate another important feature of the aQGC contributions, namely, the polarization of the  $W$  boson and the resulting angular distribution of the leptons. The polarization of the  $W$  and  $Z$  bosons plays an important role in testing the SM [50]. Angular distribution is a good observable to search for BSM signals (an excellent example is the  $P'_5$  form factor [51, 52]) because the differential cross section exposes more information than the total cross section. Although the polarization fractions of the  $W$  and  $Z$  bosons have been studied extensively within the SM [53-58], the angular distribution caused by the polarization effects of aQGCs needs further investigation.

The paper is organized as follows: in section 2, we introduce the effective Lagrangian and the corresponding dimension-8 anomalous quartic gauge-boson operators relevant to  $W\gamma jj$  production in VBS processes, and the experimental constraints on these operators are presented. In section 3, we analyze the partial-wave unitarity bounds. In section 4, we first propose a cut based on the unitarity bound to ensure that the selected events are described correctly using the SMEFT. Next, we discuss the kinematic and polarization features of the signal events as well as the event selection strategy. Based on our event selection strategy, we obtain the constraints on the coefficients of dimension-8 operators with current luminosity at the LHC. In section 5, we present the cross sections and the significance of the aQGC signals in the  $\ell\nu\gamma jj$  final state. Finally, we summarize our results in section 6.

## 2 Operator basis and constraints from experiments

The Lagrangian of the SMEFT can be written in terms of an expansion in powers of the inverse of new physics scale  $\Lambda$  [4-6]:

$$\mathcal{L}_{\text{SMEFT}} = \mathcal{L}_{\text{SM}} + \sum_i \frac{C_{6i}}{\Lambda^2} O_{6i} + \sum_j \frac{C_{8j}}{\Lambda^4} O_{8j} + \dots, \quad (1)$$

where  $O_{6i}$  and  $O_{8j}$  are dimension-6 and dimension-8 operators, respectively, and  $C_{6i}/\Lambda^2$  and  $C_{8j}/\Lambda^4$  are the corresponding Wilson coefficients. The effects of BSM are described by higher dimensional operators, which are suppressed by  $\Lambda$ . For one generation fermions, 86 independent operators, out of 895 baryon number conserving dimension-8 operators, can contribute to QGCs and TGCs [22].

We list dimension-8 operators affecting the aQGCs

relevant to the  $W\gamma jj$  production [59, 60]:

$$\mathcal{L}_{\text{aQGC}} = \sum_j \frac{f_{M_j}}{\Lambda^4} O_{M_j} + \sum_k \frac{f_{T_k}}{\Lambda^4} O_{T_k}, \quad (2)$$

with

$$\begin{aligned} O_{M_0} &= \text{Tr}[\widehat{W}_{\mu\nu} \widehat{W}^{\mu\nu}] \times \left[ (D^\beta \Phi)^\dagger D^\beta \Phi \right], \\ O_{M_1} &= \text{Tr}[\widehat{W}_{\mu\nu} \widehat{W}^{\nu\beta}] \times \left[ (D^\beta \Phi)^\dagger D^\mu \Phi \right], \\ O_{M_2} &= [B_{\mu\nu} B^{\mu\nu}] \times \left[ (D^\beta \Phi)^\dagger D^\beta \Phi \right], \\ O_{M_3} &= [B_{\mu\nu} B^{\nu\beta}] \times \left[ (D^\beta \Phi)^\dagger D^\mu \Phi \right], \\ O_{M_4} &= \left[ (D_\mu \Phi)^\dagger \widehat{W}_{\beta\nu} D^\mu \Phi \right] \times B^{\beta\nu}, \\ O_{M_5} &= \left[ (D_\mu \Phi)^\dagger \widehat{W}_{\beta\nu} D_\nu \Phi \right] \times B^{\beta\mu} + \text{h.c.}, \\ O_{M_7} &= (D_\mu \Phi)^\dagger \widehat{W}_{\beta\nu} \widehat{W}_{\beta\mu} D_\nu \Phi, \\ O_{T_0} &= \text{Tr}[\widehat{W}_{\mu\nu} \widehat{W}^{\mu\nu}] \times \text{Tr}[\widehat{W}_{\alpha\beta} \widehat{W}^{\alpha\beta}], \\ O_{T_1} &= \text{Tr}[\widehat{W}_{\alpha\nu} \widehat{W}^{\mu\beta}] \times \text{Tr}[\widehat{W}_{\mu\beta} \widehat{W}^{\alpha\nu}], \\ O_{T_2} &= \text{Tr}[\widehat{W}_{\alpha\mu} \widehat{W}^{\mu\beta}] \times \text{Tr}[\widehat{W}_{\beta\nu} \widehat{W}^{\nu\alpha}], \\ O_{T_5} &= \text{Tr}[\widehat{W}_{\mu\nu} \widehat{W}^{\mu\nu}] \times B_{\alpha\beta} B^{\alpha\beta}, \\ O_{T_6} &= \text{Tr}[\widehat{W}_{\alpha\nu} \widehat{W}^{\mu\beta}] \times B_{\mu\beta} B^{\alpha\nu}, \\ O_{T_7} &= \text{Tr}[\widehat{W}_{\alpha\mu} \widehat{W}^{\mu\beta}] \times B_{\beta\nu} B^{\nu\alpha}, \end{aligned} \quad (3)$$

where  $\widehat{W} \equiv \vec{\sigma} \cdot \vec{W}/2$ ,  $\sigma$  is the Pauli matrix, and  $\vec{W} \equiv \{W^1, W^2, W^3\}$ .

The tightest constraints on the coefficients of the corresponding operators are obtained via  $WWjj$ ,  $WZjj$ ,  $ZZjj$ , and  $Z\gamma jj$  channels through CMS experiments at  $\sqrt{s} = 13$  TeV [61, 62], which are listed in Table 1.

Table 1. Constraints on coefficients obtained through CMS experiments.

coefficient	constraint	coefficient	constraint
$f_{M_0}/\Lambda^4$ (TeV <sup>-4</sup> )	[-0.69, 0.70] [61]	$f_{T_0}/\Lambda^4$ (TeV <sup>-4</sup> )	[-0.12, 0.11] [61]
$f_{M_1}/\Lambda^4$ (TeV <sup>-4</sup> )	[-2.0, 2.1] [61]	$f_{T_1}/\Lambda^4$ (TeV <sup>-4</sup> )	[-0.12, 0.13] [61]
$f_{M_2}/\Lambda^4$ (TeV <sup>-4</sup> )	[-8.2, 8.0] [62]	$f_{T_2}/\Lambda^4$ (TeV <sup>-4</sup> )	[-0.28, 0.28] [61]
$f_{M_3}/\Lambda^4$ (TeV <sup>-4</sup> )	[-21, 21] [62]	$f_{T_5}/\Lambda^4$ (TeV <sup>-4</sup> )	[-0.7, 0.74] [62]
$f_{M_4}/\Lambda^4$ (TeV <sup>-4</sup> )	[-15, 16] [62]	$f_{T_6}/\Lambda^4$ (TeV <sup>-4</sup> )	[-1.6, 1.7] [62]
$f_{M_5}/\Lambda^4$ (TeV <sup>-4</sup> )	[-25, 24] [62]	$f_{T_7}/\Lambda^4$ (TeV <sup>-4</sup> )	[-2.6, 2.8] [62]
$f_{M_7}/\Lambda^4$ (TeV <sup>-4</sup> )	[-3.4, 3.4] [61]		

The aQGC vertices relevant to the  $W\gamma jj$  channel are  $W^+W^-\gamma\gamma$  and  $W^+W^-Z\gamma$ , which are

$$\begin{aligned} V_{WWZ\gamma,0} &= F^{\mu\alpha} Z_{\mu\beta} (W_\alpha^+ W^{-\beta} + W_\alpha^- W^{+\beta}), \\ V_{WWZ\gamma,1} &= F^{\mu\alpha} Z_\alpha (W_{\mu\beta}^+ W^{-\beta} + W_{\mu\beta}^- W^{+\beta}), \end{aligned}$$

$$\begin{aligned} V_{WWZ\gamma,2} &= F^{\mu\nu} Z_{\mu\nu} W_\alpha^+ W^{-\alpha}, \\ V_{WWZ\gamma,3} &= F^{\mu\alpha} Z^\beta (W_{\mu\alpha}^+ W_\beta^- + W_{\mu\alpha}^- W_\beta^+), \\ V_{WWZ\gamma,4} &= F^{\mu\alpha} Z^\beta (W_{\mu\beta}^+ W_\alpha^- + W_{\mu\beta}^- W_\alpha^+), \\ V_{WWZ\gamma,5} &= F^{\mu\nu} Z_{\mu\nu} W^{+\alpha\beta} W_{\alpha\beta}^-, \\ V_{WWZ\gamma,6} &= F^{\mu\alpha} Z_{\mu\beta} (W_{\nu\alpha}^+ W^{-\nu\beta} + W_{\nu\alpha}^- W^{+\nu\beta}), \\ V_{WWZ\gamma,7} &= F^{\mu\nu} Z^{\alpha\beta} (W_{\mu\nu}^+ W_{\alpha\beta}^- + W_{\mu\nu}^- W_{\alpha\beta}^+). \end{aligned} \quad (5)$$

$$\begin{aligned} V_{WW\gamma\gamma,0} &= F_{\mu\nu} F^{\mu\nu} W^+\alpha W_\alpha^-, \quad V_{WW\gamma\gamma,1} = F_{\mu\nu} F^{\mu\alpha} W^{+\nu} W_\alpha^-, \\ V_{WW\gamma\gamma,2} &= F_{\mu\nu} F^{\mu\nu} W_{\alpha\beta}^+ W^{-\alpha\beta}, \quad V_{WW\gamma\gamma,3} = F_{\mu\nu} F^{\nu\alpha} W_{\alpha\beta}^+ W^{-\beta\mu}, \\ V_{WW\gamma\gamma,4} &= F_{\mu\nu} F^{\alpha\beta} W_{\mu\nu}^+ W^{-\alpha\beta}, \end{aligned} \quad (6)$$

and the coefficients are

$$\begin{aligned} \alpha_{WWZ\gamma,0} &= \frac{e^2 v^2}{8\Lambda^4} \left( \frac{c_W^2}{s_W^2} f_{M_5} - f_{M_5} - \frac{c_W}{s_W} f_{M_1} + 2 \frac{c_W}{s_W} f_{M_3} + \frac{c_W}{2s_W} f_{M_7} \right), \\ \alpha_{WWZ\gamma,1} &= \frac{e^2 v^2}{8\Lambda^4} \left( -\frac{1}{2} \left( \frac{c_W}{s_W} + \frac{s_W}{c_W} \right) f_{M_7} - f_{M_5} - \frac{c_W^2}{s_W^2} f_{M_5} \right), \\ \alpha_{WWZ\gamma,2} &= \frac{e^2 v^2}{8\Lambda^4} \left( \frac{c_W^2}{s_W^2} f_{M_4} - f_{M_4} + 2 \frac{c_W}{s_W} f_{M_0} - 4 \frac{c_W}{s_W} f_{M_2} \right), \\ \alpha_{WWZ\gamma,3} &= \frac{e^2 v^2}{8\Lambda^4} \left( -\frac{c_W^2}{s_W^2} f_{M_4} - f_{M_4} \right), \\ \alpha_{WWZ\gamma,4} &= \frac{e^2 v^2}{8\Lambda^4} \left( \frac{1}{2} \left( \frac{c_W}{s_W} + \frac{s_W}{c_W} \right) f_{M_7} - f_{M_5} - \frac{c_W^2}{s_W^2} f_{M_5} \right), \\ \alpha_{WWZ\gamma,5} &= \frac{2c_W s_W}{\Lambda^4} (f_{T_0} - f_{T_5}), \\ \alpha_{WWZ\gamma,6} &= \frac{c_W s_W}{\Lambda^4} (f_{T_2} - f_{T_7}), \\ \alpha_{WWZ\gamma,7} &= \frac{c_W s_W}{\Lambda^4} (f_{T_1} - f_{T_6}), \\ \alpha_{WW\gamma\gamma,0} &= \frac{e^2 v^2}{8\Lambda^4} \left( f_{M_0} + \frac{c_W}{s_W} f_{M_4} + 2 \frac{c_W^2}{s_W^2} f_{M_2} \right), \\ \alpha_{WW\gamma\gamma,1} &= \frac{e^2 v^2}{8\Lambda^4} \left( \frac{1}{2} f_{M_7} + 2 \frac{c_W}{s_W} f_{M_5} - f_{M_1} - 2 \frac{c_W^2}{s_W^2} f_{M_5} \right), \\ \alpha_{WW\gamma\gamma,2} &= \frac{1}{\Lambda^4} (s_W^2 f_{T_0} + c_W^2 f_{T_5}), \quad \alpha_{WW\gamma\gamma,3} = \frac{1}{\Lambda^4} (s_W^2 f_{T_2} + c_W^2 f_{T_7}), \\ \alpha_{WW\gamma\gamma,4} &= \frac{1}{\Lambda^4} (s_W^2 f_{T_1} + c_W^2 f_{T_6}). \end{aligned} \quad (7)$$

Note that vertices  $V_{WWZ\gamma,0,1,2,3,4}$  and  $V_{AAWW,0,1}$  are dimension-6 derived from  $O_{M_i}$ , and the other vertices are dimension-8 derived from  $O_{T_i}$ .

### 3 Unitarity bounds

Unlike in the SM, the cross section of the VBS process with aQGCs increases with c.m. energy. Such a feature opens a window to detect aQGCs at higher energies. However, the cross section with aQGCs will violate unit-

arity at a certain energy scale. The unitarity violation indicates that the SMEFT is no longer appropriate for describing the phenomenon at such high energies perturbatively.

Considering the process  $V_{1,\lambda_1} V_{2,\lambda_2} \rightarrow V_{3,\lambda_3} V_{4,\lambda_4}$ , where  $V_i$  are vector bosons,  $\lambda_i$  correspond to the helicities of  $V_i$ , and therefore  $\lambda_i = \pm 1$  for photons, and  $\lambda_i = \pm 1, 0$  for  $W^\pm, Z$  bosons, its amplitudes can be expanded as [63, 64]

$$\begin{aligned} \mathcal{M}(V_{1,\lambda_1} W_{\lambda_2}^+ \rightarrow \gamma_{\lambda_3} W_{\lambda_4}^+) = & 8\pi \sum_J (2J+1) \sqrt{1+\delta_{\lambda_1,\lambda_2}} \\ & \times \sqrt{1+\delta_{\lambda_3,\lambda_4}} e^{i(\lambda-\lambda')\varphi} d_{\lambda,\lambda'}^J(\theta) T^J, \quad (9) \end{aligned}$$

where  $V_1$  is  $\gamma$  or  $Z$  boson,  $\lambda = \lambda_1 - \lambda_2$ ,  $\lambda' = \lambda_3 - \lambda_4$ ,  $\theta$  and  $\phi$  are the zenith and azimuth angles of the  $\gamma$  in the final state,  $d_{\lambda,\lambda'}^J(\theta)$  are the Wigner  $d$ -functions [63], and  $T^J$  are coefficients of the expansion that can be obtained via Eq. (9). Partial-wave unitarity for the elastic channels requires  $|T^J| \leq 2$  [64], which has been used widely in previous studies [65–68].

### 3.1 Partial-wave expansions of the $W\gamma \rightarrow W\gamma$ amplitudes

We calculate the partial-wave expansions of the  $W\gamma \rightarrow W\gamma$  amplitudes with one dimension-8 operator at a

time. Denoting  $\mathcal{M}^{f_x}$  as the amplitude with only the  $O_X$  operator, for  $O_{M_{2,3,4,5,7}}$  and  $O_{T_{5,6,7}}$ , which can be derived using Eq. (8) as

$$\begin{aligned} \mathcal{M}^{f_{M_1}}(W^+\gamma \rightarrow W^+\gamma) &= \frac{c_W}{s_W} \frac{f_{M_1}}{f_{M_0}} \mathcal{M}^{f_{M_0}}(W^+\gamma \rightarrow W^+\gamma), \\ \mathcal{M}^{f_{M_2}}(W^+\gamma \rightarrow W^+\gamma) &= \frac{2c_W^2}{s_W^2} \frac{f_{M_2}}{f_{M_0}} \mathcal{M}^{f_{M_0}}(W^+\gamma \rightarrow W^+\gamma), \\ \mathcal{M}^{f_{M_3}}(W^+\gamma \rightarrow W^+\gamma) &= \frac{2c_W^2}{s_W^2} \frac{f_{M_3}}{f_{M_1}} \mathcal{M}^{f_{M_1}}(W^+\gamma \rightarrow W^+\gamma), \\ \mathcal{M}^{f_{M_5}}(W^+\gamma \rightarrow W^+\gamma) &= -\frac{2c_W}{s_W} \frac{f_{M_5}}{f_{M_1}} \mathcal{M}^{f_{M_1}}(W^+\gamma \rightarrow W^+\gamma), \\ \mathcal{M}^{f_{M_7}}(W^+\gamma \rightarrow W^+\gamma) &= -\frac{1}{2} \frac{f_{M_7}}{f_{M_1}} \mathcal{M}^{f_{M_1}}(W^+\gamma \rightarrow W^+\gamma), \\ \mathcal{M}^{f_{T_5}}(W^+\gamma \rightarrow W^+\gamma) &= \frac{c_W^2}{s_W^2} \frac{f_{T_5}}{f_{T_0}} \mathcal{M}^{f_{T_0}}(W^+\gamma \rightarrow W^+\gamma), \\ \mathcal{M}^{f_{T_6}}(W^+\gamma \rightarrow W^+\gamma) &= \frac{c_W^2}{s_W^2} \frac{f_{T_6}}{f_{T_1}} \mathcal{M}^{f_{T_1}}(W^+\gamma \rightarrow W^+\gamma), \\ \mathcal{M}^{f_{T_7}}(W^+\gamma \rightarrow W^+\gamma) &= \frac{c_W^2}{s_W^2} \frac{f_{T_7}}{f_{T_2}} \mathcal{M}^{f_{T_2}}(W^+\gamma \rightarrow W^+\gamma). \quad (10) \end{aligned}$$

Therefore, only the partial-wave expansions of amplitudes for the  $O_{M_{0,1}}$  and  $O_{T_{0,1,2}}$  operators are required to be

Table 2. Partial-wave expansions of  $W\gamma \rightarrow W\gamma$  amplitudes with one of dimension-8 operators  $O_{M_{0,1}}$  and  $O_{T_{0,1,2}}$  at the leading order. The amplitudes that set the strongest bounds are marked using an '\*'.  $\theta$  and  $\varphi$  are zenith and azimuth angles of  $\gamma$  in the final state.

amplitudes	leading order	expansions
$\mathcal{M}(\gamma_+ W_0^+ \rightarrow \gamma_- W_0^+)$	$-\frac{f_{M_0}}{\Lambda^4} \frac{e^2 e^{i\varphi} v^2 \sin^4\left(\frac{\theta}{2}\right)}{8M_W^2} \delta^2$ $\frac{f_{M_1}}{\Lambda^4} \frac{e^2 e^{i\varphi} v^2 \sin^4\left(\frac{\theta}{2}\right)}{32M_W^2} \delta^2$	$-\frac{f_{M_0}}{\Lambda^4} \frac{e^2 e^{2i\varphi} v^2}{8M_W^2} \delta^2 \left(\frac{3}{4} d_{1,-1}^1 - \frac{1}{4} d_{1,-1}^2\right)^*$ $\frac{f_{M_1}}{\Lambda^4} \frac{e^2 e^{2i\varphi} v^2}{32M_W^2} \delta^2 \left(\frac{3}{4} d_{1,-1}^1 - \frac{1}{4} d_{1,-1}^2\right)$
$\mathcal{M}(\gamma_+ W_0^+ \rightarrow \gamma_+ W_0^+)$	$\frac{f_{M_1}}{\Lambda^4} \frac{e^2 e^{i\varphi} v^2 (\cos(\theta) + 1)}{32M_W^2} \delta^2$	$\frac{f_{M_1}}{\Lambda^4} \frac{e^2 v^2}{16M_W^2} \delta^2 d_{1,1}^1 *$
$\mathcal{M}(\gamma_+ W_+^+ \rightarrow \gamma_- W_+^+)$	$2 \frac{f_{T_0}}{\Lambda^4} s_W^2 \sin^4\left(\frac{\theta}{2}\right) \delta^2$ $\frac{1}{2} \frac{f_{T_1}}{\Lambda^4} s_W^2 \left(\sin^4\left(\frac{\theta}{2}\right) + \left(\frac{\cos(\theta)+3}{2}\right)^2\right) \delta^2$ $\frac{1}{2} \frac{f_{T_2}}{\Lambda^4} s_W^2 \sin^4\left(\frac{\theta}{2}\right) \delta^2$	$2 \frac{f_{T_0}}{\Lambda^4} s_W^2 \delta^2 \left(\frac{1}{3} d_{0,0}^0 - \frac{1}{2} d_{0,0}^1 + \frac{1}{6} d_{0,0}^2\right)$ $\frac{1}{2} \frac{f_{T_1}}{\Lambda^4} s_W^2 \delta^2 (-2d_{0,0}^0 - 2d_{0,0}^1) *$ $\frac{1}{2} \frac{f_{T_2}}{\Lambda^4} s_W^2 \delta^2 \left(\frac{1}{3} d_{0,0}^0 - \frac{1}{2} d_{0,0}^1 + \frac{1}{6} d_{0,0}^2\right)$
$\mathcal{M}(\gamma_+ W_-^+ \rightarrow \gamma_- W_-^+)$	$2 \frac{f_{T_0}}{\Lambda^4} e^{2i\varphi} s_W^2 \sin^4\left(\frac{\theta}{2}\right) \delta^2$ $\frac{1}{2} \frac{f_{T_2}}{\Lambda^4} e^{2i\varphi} s_W^2 \sin^4\left(\frac{\theta}{2}\right) \delta^2$	$2 \frac{f_{T_0}}{\Lambda^4} e^{4i\varphi} s_W^2 \delta^2 d_{2,-2}^2 *$ $\frac{1}{2} \frac{f_{T_2}}{\Lambda^4} e^{4i\varphi} s_W^2 \delta^2 d_{2,-2}^2$
$\mathcal{M}(\gamma_- W_-^+ \rightarrow \gamma_- W_-^+)$	$\frac{f_{T_1}}{\Lambda^4} s_W^2 \delta^2$ $\frac{1}{2} \frac{f_{T_2}}{\Lambda^4} s_W^2 \delta^2$	$\frac{f_{T_1}}{\Lambda^4} s_W^2 \delta^2 d_{0,0}^0 *$ $\frac{1}{2} \frac{f_{T_2}}{\Lambda^4} s_W^2 \delta^2 d_{0,0}^0 *$
$\mathcal{M}(\gamma_+ W_-^+ \rightarrow \gamma_+ W_-^+)$	$\frac{f_{T_1}}{\Lambda^4} e^{2i\varphi} s_W^2 \cos^4\left(\frac{\theta}{2}\right) \delta^2$ $\frac{1}{2} \frac{f_{T_2}}{\Lambda^4} e^{2i\varphi} s_W^2 \cos^4\left(\frac{\theta}{2}\right) \delta^2$	$\frac{f_{T_1}}{\Lambda^4} s_W^2 \delta^2 d_{2,2}^2$ $\frac{1}{2} \frac{f_{T_2}}{\Lambda^4} s_W^2 \delta^2 d_{2,2}^2$

calculated. The amplitudes increase with the c.m. energy  $\sqrt{s}$ . Retaining only the leading terms, the results are listed in Table 2. There are also leading terms that can be obtained using the relation  $\mathcal{M}_{\lambda_1, \lambda_2, \lambda_3, \lambda_4}(\theta) = (-1)^{\lambda_1 - \lambda_2 - \lambda_3 + \lambda_4} \mathcal{M}_{-\lambda_1, -\lambda_2, -\lambda_3, -\lambda_4}(\theta)$ ; however, they are not presented.

In Table 2, the channels with the largest  $|T_J|$  are marked using \*. From Table 2 and Eq. (10), we obtain the strongest bounds as

$$\begin{aligned} \left| \frac{f_{M_0}}{\Lambda^4} \right| &\leq \frac{512\pi M_W^2}{\hat{s}^2 e^2 v^2}, & \left| \frac{f_{M_1}}{\Lambda^4} \right| &\leq \frac{768\pi M_W^2}{e^2 v^2 \hat{s}^2}, \\ \left| \frac{f_{M_2}}{\Lambda^4} \right| &\leq \frac{s_W^2 256\pi M_W^2}{c_W^2 e^2 v^2 \hat{s}^2}, & \left| \frac{f_{M_3}}{\Lambda^4} \right| &\leq \frac{384 s_W^2 \pi M_W^2}{e^2 v^2 c_W^2 \hat{s}^2}, \\ \left| \frac{f_{M_4}}{\Lambda^4} \right| &\leq \frac{s_W 512\pi M_W^2}{c_W e^2 v^2 \hat{s}^2}, & \left| \frac{f_{M_5}}{\Lambda^4} \right| &\leq \frac{384 s_W \pi M_W^2}{e^2 v^2 c_W \hat{s}^2}, \\ \left| \frac{f_{M_7}}{\Lambda^4} \right| &\leq \frac{1536\pi M_W^2}{e^2 v^2 \hat{s}^2}, & \left| \frac{f_{T_0}}{\Lambda^4} \right| &\leq \frac{40\pi}{s_W^2 \hat{s}^2}, \\ \left| \frac{f_{T_1}}{\Lambda^4} \right| &\leq \frac{32\pi}{s_W^2 \hat{s}^2}, & \left| \frac{f_{T_2}}{\Lambda^4} \right| &\leq \frac{64\pi}{s_W^2 \hat{s}^2}, \end{aligned}$$

$$\left| \frac{f_{T_5}}{\Lambda^4} \right| \leq \frac{40\pi}{c_W^2 \hat{s}^2}, \quad \left| \frac{f_{T_6}}{\Lambda^4} \right| \leq \frac{32\pi}{c_W^2 \hat{s}^2}, \quad \left| \frac{f_{T_7}}{\Lambda^4} \right| \leq \frac{64\pi}{c_W^2 \hat{s}^2}. \quad (11)$$

### 3.2 Partial-wave expansions of $WZ \rightarrow W\gamma$ amplitudes

For  $WZ \rightarrow W\gamma$ , similarly,

$$\begin{aligned} \mathcal{M}^{f_{M_2}}(W^+Z \rightarrow W^+\gamma) &= -2 \frac{f_{M_2}}{f_{M_0}} \mathcal{M}^{f_{M_0}}(W^+Z \rightarrow W^+\gamma), \\ \mathcal{M}^{f_{M_3}}(W^+Z \rightarrow W^+\gamma) &= -2 \frac{f_{M_3}}{f_{M_1}} \mathcal{M}^{f_{M_1}}(W^+Z \rightarrow W^+\gamma), \\ \mathcal{M}^{f_{T_5}}(W^+Z \rightarrow W^+\gamma) &= -\frac{f_{T_5}}{f_{T_0}} \mathcal{M}^{f_{T_0}}(W^+Z \rightarrow W^+\gamma), \\ \mathcal{M}^{f_{T_6}}(W^+Z \rightarrow W^+\gamma) &= -\frac{f_{T_6}}{f_{T_1}} \mathcal{M}^{f_{T_1}}(W^+Z \rightarrow W^+\gamma), \\ \mathcal{M}^{f_{T_7}}(W^+Z \rightarrow W^+\gamma) &= -\frac{f_{T_7}}{f_{T_2}} \mathcal{M}^{f_{T_2}}(W^+Z \rightarrow W^+\gamma). \end{aligned} \quad (12)$$

The partial-wave expansions for the amplitudes of  $O_{M_{0,1,4,5,7}}$  and  $O_{T_{0,1,2}}$  are listed in Table 3. The strongest bounds can be obtained via Table 3 and Eq. (12),

Table 3. Same as Table 2 but for  $WZ \rightarrow W\gamma$ .

amplitudes	leading order	expansions
$\mathcal{M}(Z_+ W_0^+ \rightarrow \gamma_- W_0^+)$	$-\frac{f_{M_0}}{\Lambda^4} \frac{c_W e^2 e^{i\varphi} v^2 \sin^4\left(\frac{\theta}{2}\right)}{8M_W^2 s_W} \hat{s}^2$	$-\frac{f_{M_0}}{\Lambda^4} \frac{c_W e^2 e^{2i\varphi} v^2}{8M_W^2 s_W} \hat{s}^2 \left(\frac{3}{4} d_{1,-1}^1 - \frac{1}{4} d_{1,-1}^2\right)^*$
	$\frac{f_{M_1}}{\Lambda^4} \frac{c_W e^2 e^{i\varphi} v^2 \sin^4\left(\frac{\theta}{2}\right)}{32M_W^2 s_W} \hat{s}^2$	$\frac{f_{M_1}}{\Lambda^4} \frac{c_W e^2 e^{2i\varphi} v^2}{32M_W^2 s_W} \hat{s}^2 \left(\frac{3}{4} d_{1,-1}^1 - \frac{1}{4} d_{1,-1}^2\right)$
	$\frac{f_{M_4}}{\Lambda^4} \frac{e^2 e^{i\varphi} v^2 (s_W^2 - c_W^2) \sin^4\left(\frac{\theta}{2}\right)}{16M_W^2 c_W^2} \hat{s}^2$	$\frac{f_{M_4}}{\Lambda^4} \frac{e^2 e^{2i\varphi} v^2 (s_W^2 - c_W^2)}{16M_W^2 c_W^2} \hat{s}^2 \left(\frac{3}{4} d_{1,-1}^1 - \frac{1}{4} d_{1,-1}^2\right)$
	$\frac{f_{M_5}}{\Lambda^4} \frac{e^2 e^{i\varphi} v^2 (s_W^2 - c_W^2) \sin^4\left(\frac{\theta}{2}\right)}{32M_W^2 s_W^2} \hat{s}^2$	$\frac{f_{M_5}}{\Lambda^4} \frac{e^2 e^{2i\varphi} v^2 (s_W^2 - c_W^2)}{32M_W^2 s_W^2} \hat{s}^2 \left(\frac{3}{4} d_{1,-1}^1 - \frac{1}{4} d_{1,-1}^2\right)$
	$-\frac{f_{M_7}}{\Lambda^4} \frac{c_W e^2 e^{i\varphi} v^2 \sin^4\left(\frac{\theta}{2}\right)}{64M_W^2 s_W} \hat{s}^2$	$-\frac{f_{M_7}}{\Lambda^4} \frac{c_W e^2 e^{2i\varphi} v^2}{64M_W^2 s_W} \hat{s}^2 \left(\frac{3}{4} d_{1,-1}^1 - \frac{1}{4} d_{1,-1}^2\right)$
$\mathcal{M}(Z_+ W_0^+ \rightarrow \gamma_+ W_0^+)$	$\frac{f_{M_1}}{\Lambda^4} \frac{c_W e^2 e^{i\varphi} v^2 \cos^2\left(\frac{\theta}{2}\right)}{16M_W^2 s_W} \hat{s}^2$	$\frac{f_{M_1}}{\Lambda^4} \frac{c_W e^2 v^2}{16M_W^2 s_W} \hat{s}^2 d_{1,1}^2$ *
	$\frac{f_{M_5}}{\Lambda^4} \frac{e^2 e^{i\varphi} v^2 (s_W^2 - c_W^2) \cos^2\left(\frac{\theta}{2}\right)}{16M_W^2 s_W^2} \hat{s}^2$	$\frac{f_{M_5}}{\Lambda^4} \frac{e^2 v^2 (s_W^2 - c_W^2)}{16M_W^2 s_W^2} \hat{s}^2 d_{1,1}^1$
	$-\frac{f_{M_7}}{\Lambda^4} \frac{c_W e^2 e^{i\varphi} v^2 \cos^2\left(\frac{\theta}{2}\right)}{32M_W^2 s_W} \hat{s}^2$	$-\frac{f_{M_7}}{\Lambda^4} \frac{c_W e^2 v^2}{32M_W^2 s_W} \hat{s}^2 d_{1,1}^1$ *
$\mathcal{M}(Z_0 W_+^+ \rightarrow \gamma_- W_0^+)$	$\frac{f_{M_4}}{\Lambda^4} \frac{e^2 e^{-i\varphi} v^2 \cos^4\left(\frac{\theta}{2}\right)}{16M_W M_Z s_W^2} \hat{s}^2$	$\frac{f_{M_4}}{\Lambda^4} \frac{e^2 v^2}{64M_W M_Z s_W^2} \hat{s}^2 (3d_{-1,-1}^1 + d_{-1,-1}^2)$
	$\frac{f_{M_5}}{\Lambda^4} \frac{e^2 e^{-i\varphi} v^2 \cos^4\left(\frac{\theta}{2}\right)}{32M_W M_Z s_W^2} \hat{s}^2$	$\frac{f_{M_5}}{\Lambda^4} \frac{e^2 v^2}{128M_W M_Z s_W^2} \hat{s}^2 (3d_{-1,-1}^1 + d_{-1,-1}^2)$
	$\frac{f_{M_7}}{\Lambda^4} \frac{e^2 e^{-i\varphi} v^2 \cos^2\left(\frac{\theta}{2}\right) (\cos\theta - 3)}{128c_W s_W M_W M_Z} \hat{s}^2$	$\frac{f_{M_7}}{\Lambda^4} \frac{e^2 v^2}{256c_W s_W M_W M_Z} \hat{s}^2 (-5d_{-1,-1}^1 + d_{-1,-1}^2)$

Continued on next page

Table 3-continued from previous page

amplitudes	leading order	expansions
$M(Z_0 W_0^+ \rightarrow \gamma_+ W_+^+)$	$\frac{f_{M_4}}{\Lambda^4} \frac{e^2 v^2}{16 M_W M_Z s_W^2} \hat{s}^2$ $\frac{f_{M_5}}{\Lambda^4} \frac{e^2 v^2}{32 M_W M_Z s_W^2} \hat{s}^2$ $-\frac{f_{M_7}}{\Lambda^4} \frac{e^2 v^2 \cos(\theta)}{64 c_W s_W M_W M_Z} \hat{s}^2$	$\frac{f_{M_4}}{\Lambda^4} \frac{e^2 v^2}{16 M_W M_Z s_W^2} \hat{s}^2 d_{0,0}^0 *$ $\frac{f_{M_5}}{\Lambda^4} \frac{e^2 v^2}{32 M_W M_Z s_W^2} \hat{s}^2 d_{0,0}^0 *$ $-\frac{f_{M_7}}{\Lambda^4} \frac{e^2 v^2}{64 c_W s_W M_W M_Z} \hat{s}^2 d_{0,0}^1$
$M(Z_0 W_0^+ \rightarrow \gamma_+ W_-^+)$	$-\frac{f_{M_5}}{\Lambda^4} \frac{e^2 v^2 \sin^2(\theta)}{64 M_W M_Z s_W^2} \hat{s}^2$	$-\frac{f_{M_5}}{\Lambda^4} \frac{e^2 v^2 e^{-2i\varphi}}{32 M_W M_Z s_W^2} \hat{s}^2 \sqrt{\frac{2}{3}} d_{0,2}^0$
$M(Z_+ W_+^+ \rightarrow \gamma_- W_-^+)$	$2 \frac{f_{T_0}}{\Lambda^4} c_W s_W \sin^4\left(\frac{\theta}{2}\right) \hat{s}^2$ $\frac{f_{T_1}}{\Lambda^4} c_W s_W \frac{4 \cos(\theta) + \cos(2\theta) + 11}{8} \hat{s}^2$ $\frac{f_{T_2}}{\Lambda^4} c_W s_W \frac{\cos(2\theta) - 4 \cos(\theta) + 3}{16} \hat{s}^2$	$2 \frac{f_{T_0}}{\Lambda^4} c_W s_W \hat{s}^2 \left( \frac{1}{3} d_{0,0}^0 - \frac{1}{2} d_{0,0}^1 + \frac{1}{6} d_{0,0}^2 \right)$ $\frac{1}{2} \frac{f_{T_1}}{\Lambda^4} c_W s_W \hat{s}^2 \left( \frac{8}{3} d_{0,0}^0 + d_{0,0}^1 + \frac{1}{3} d_{0,0}^2 \right) *$ $\frac{1}{4} \frac{f_{T_2}}{\Lambda^4} c_W s_W \hat{s}^2 \left( \frac{2}{3} d_{0,0}^0 - d_{0,0}^1 + \frac{1}{3} d_{0,0}^2 \right)$
$M(Z_+ W_-^+ \rightarrow \gamma_- W_+^+)$	$2 \frac{f_{T_0}}{\Lambda^4} c_W s_W e^{2i\varphi} \sin^4\left(\frac{\theta}{2}\right) \hat{s}^2$ $\frac{1}{2} \frac{f_{T_2}}{\Lambda^4} c_W s_W e^{2i\varphi} \sin^4\left(\frac{\theta}{2}\right) \hat{s}^2$	$2 \frac{f_{T_0}}{\Lambda^4} c_W s_W e^{4i\varphi} \hat{s}^2 d_{2,-2}^2 *$ $\frac{1}{2} \frac{f_{T_2}}{\Lambda^4} c_W s_W e^{4i\varphi} \hat{s}^2 d_{2,-2}^2$
$M(Z_+ W_+^+ \rightarrow \gamma_+ W_+^+)$	$\frac{f_{T_1}}{\Lambda^4} c_W s_W \hat{s}^2$ $\frac{1}{2} \frac{f_{T_2}}{\Lambda^4} c_W s_W \hat{s}^2$	$\frac{f_{T_1}}{\Lambda^4} c_W s_W \hat{s}^2 d_{0,0}^0$ $\frac{1}{2} \frac{f_{T_2}}{\Lambda^4} c_W s_W \hat{s}^2 d_{0,0}^0 *$
$M(Z_+ W_-^+ \rightarrow \gamma_+ W_-^+)$	$\frac{f_{T_1}}{\Lambda^4} c_W s_W e^{2i\varphi} \cos^4\left(\frac{\theta}{2}\right) \hat{s}^2$ $\frac{1}{2} \frac{f_{T_2}}{\Lambda^4} c_W s_W e^{2i\varphi} \cos^4\left(\frac{\theta}{2}\right) \hat{s}^2$	$\frac{f_{T_1}}{\Lambda^4} c_W s_W \hat{s}^2 d_{2,2}^2$ $\frac{1}{2} \frac{f_{T_2}}{\Lambda^4} c_W s_W \hat{s}^2 d_{2,2}^2$

$$\begin{aligned}
 \left| \frac{f_{M_0}}{\Lambda^4} \right| &\leq \frac{512\pi M_W^2 s_W}{c_W e^2 v^2 \hat{s}^2}, & \left| \frac{f_{M_1}}{\Lambda^4} \right| &\leq \frac{768\pi M_W^2 s_W}{c_W e^2 v^2 \hat{s}^2}, & \left| \frac{f_{M_0}}{\Lambda^4} \right| &\leq \frac{512\pi M_W^2 s_W}{c_W e^2 v^2 \hat{s}^2}, & \left| \frac{f_{M_1}}{\Lambda^4} \right| &\leq \frac{768\pi M_W^2 s_W}{c_W e^2 v^2 \hat{s}^2}, \\
 \left| \frac{f_{M_2}}{\Lambda^4} \right| &\leq \frac{256\pi M_W^2 s_W}{c_W e^2 v^2 \hat{s}^2}, & \left| \frac{f_{M_3}}{\Lambda^4} \right| &\leq \frac{384\pi M_W^2 s_W}{c_W e^2 v^2 \hat{s}^2}, & \left| \frac{f_{M_2}}{\Lambda^4} \right| &\leq \frac{s_W^2 256\pi M_W^2}{c_W^2 e^2 v^2 \hat{s}^2}, & \left| \frac{f_{M_3}}{\Lambda^4} \right| &\leq \frac{384\pi s_W^2 M_W^2}{c_W^2 e^2 v^2 \hat{s}^2}, \\
 \left| \frac{f_{M_4}}{\Lambda^4} \right| &\leq \frac{512\pi M_W M_Z s_W^2}{e^2 v^2 \hat{s}^2}, & \left| \frac{f_{M_5}}{\Lambda^4} \right| &\leq \frac{1024\pi M_W M_Z s_W^2}{e^2 v^2 \hat{s}^2}, & \left| \frac{f_{M_4}}{\Lambda^4} \right| &\leq \frac{512\pi M_W M_Z s_W^2}{e^2 v^2 \hat{s}^2}, & \left| \frac{f_{M_5}}{\Lambda^4} \right| &\leq \frac{384\pi M_W M_Z s_W}{c_W e^2 v^2 \hat{s}^2}, \\
 \left| \frac{f_{M_7}}{\Lambda^4} \right| &\leq \frac{1536\pi M_W^2 s_W}{e^2 v^2 c_W \hat{s}^2}, & \left| \frac{f_{T_0}}{\Lambda^4} \right| &\leq \frac{40\pi}{c_W s_W \hat{s}^2}, & \left| \frac{f_{M_7}}{\Lambda^4} \right| &\leq \frac{1536\pi s_W M_W^2}{e^2 v^2 c_W \hat{s}^2}, & \left| \frac{f_{T_0}}{\Lambda^4} \right| &\leq \frac{40\pi}{s_W c_W \hat{s}^2}, \\
 \left| \frac{f_{T_1}}{\Lambda^4} \right| &\leq \frac{24\pi}{c_W s_W \hat{s}^2}, & \left| \frac{f_{T_2}}{\Lambda^4} \right| &\leq \frac{64\pi}{c_W s_W \hat{s}^2}, & \left| \frac{f_{T_1}}{\Lambda^4} \right| &\leq \frac{24\pi}{s_W c_W \hat{s}^2}, & \left| \frac{f_{T_2}}{\Lambda^4} \right| &\leq \frac{64\pi}{s_W c_W \hat{s}^2}, \\
 \left| \frac{f_{T_5}}{\Lambda^4} \right| &\leq \frac{40\pi}{c_W s_W \hat{s}^2}, & \left| \frac{f_{T_6}}{\Lambda^4} \right| &\leq \frac{32\pi}{c_W^2 \hat{s}^2}, & \left| \frac{f_{T_5}}{\Lambda^4} \right| &\leq \frac{40\pi}{c_W^2 \hat{s}^2}, & \left| \frac{f_{T_6}}{\Lambda^4} \right| &\leq \frac{32\pi}{c_W^2 \hat{s}^2}, \\
 \left| \frac{f_{T_7}}{\Lambda^4} \right| &\leq \frac{64\pi}{c_W s_W \hat{s}^2}, & & & \left| \frac{f_{T_7}}{\Lambda^4} \right| &\leq \frac{64\pi}{c_W^2 \hat{s}^2}. & & 
 \end{aligned} \tag{13}$$

### 3.3 Partial-wave unitarity bounds

For  $W\gamma jj$  production, the process  $W\gamma \rightarrow W\gamma$  cannot be distinguished from the process  $WZ \rightarrow W\gamma$ . Therefore, we set the unitarity bounds by requiring all events to satisfy the strongest bounds. From Eqs. (11) and (13), the strongest bounds are given by

The unitarity bounds indicate that the events with a large enough  $\sqrt{\hat{s}}$  could not be described correctly by the SMEFT. The violation of unitarity can be prevented by unitarization methods such as  $K$ -matrix unitarization [69] or by putting form factors into the coefficients [19-21], as well as via dispersion relations [40, 41]. It is pointed out that the constraints on the effective couplings dependent on the method used. Therefore, one should not rely on just one-method [70]. However, in experiments, the con-

straints on the coefficients are obtained using the EFT without unitarization. To compare with the experimental data, we present our results without unitization in this paper.

In VBS processes, the initial states are protons. Therefore,  $\sqrt{\hat{s}}$  is a distribution related to the parton distribution function of a proton. One cannot set the constraints on the coefficients by  $\hat{s}$ . In this study, we discarded the events with a large  $\hat{s}$  to ensure that the events generated by the SMEFT are in the valid region. In other words, we compared the signals of aQGCs with the backgrounds under a certain energy scale cut similar to the matching procedure in Refs. [49, 71].

#### 4 Signals of aQGCs and backgrounds

The dominant signal is the leptonic decay of the  $W\gamma jj$  production induced by the dimension-8 operators. We consider one operator at a time. The Feynman diagrams are shown in Fig. 1. (a). The triboson diagrams such as Fig. 1. (b) also contribute to the signal. The typical Feynman diagrams of the SM backgrounds are shown in Fig. 2, and these are often categorized as the EW-VBS, EW-non-VBS, and QCD contributions. The triboson contribution from each  $O_{M_i}$  ( $O_{T_i}$ ) operator is two (three) orders of magnitude smaller than the dominant signal even after considering the interferences. Therefore, we concentrate on the dominant signal.

The numerical results are obtained through the Monte-Carlo (MC) simulation using the MadGraph5\_aMC@NLO (MG5) toolkit [72]. The parton distribution function is NNPDF2.3 [73]. The renormalization scale  $\mu_r$  and factorization scale  $\mu_f$  are chosen to be dynamical and are set event-by-event as  $(\prod_i^n (M_i^2 + \vec{p}_T^{(i)})^{\frac{1}{n}})$ , with  $i$  running over all heavy particles. The basic cuts are applied with the default settings of MG5 and require  $\vec{p}_T^{\gamma, \ell} > 10$  GeV,  $|\eta_{\gamma, \ell}| > 2.5$  and  $\vec{p}_T^j > 20$  GeV,  $|\eta_j| < 5$ . The events are then showered by PYTHIA8 [74] and a fast

detector simulation is performed using Delphes [75] with the CMS detector card. Jets are clustered using the anti- $k_T$  algorithm with a cone radius  $R = 0.5$  and  $\vec{p}_{T, \min} = 20$  GeV. The photon isolation uses parameter  $I_{\min}$  defined as [75]

$$I_{\min}^{\gamma} = \frac{\sum_{i \neq \gamma}^{\Delta R < \Delta R_{\max}, \vec{p}_T^i > \vec{p}_{T, \min}} \vec{p}_T^i}{\vec{p}_T^{\gamma}}, \quad (15)$$

where  $\Delta R_{\max} = 0.5$  and  $\vec{p}_{T, \min} = 0.5$  GeV, and  $I_{\min}^{\gamma} > 0.12$ . We generate the dominant signal events with the largest coefficients in Table 1. After fast detector simulation, the final states are not exactly  $\ell^+ \nu \gamma jj$ . To ensure a high quality track of the signal candidate, a minimum number of composition is required. We denote the number of jets, photons, and charged leptons as  $N_j$ ,  $N_{\gamma}$ , and  $N_{\ell^+}$ , respectively. Events are selected by requiring  $N_j \geq 2$ ,  $N_{\gamma} \geq 1$ , and  $N_{\ell^+} = 1$ . We analyze the energy scale, kinematic features, and polarization features of the events after these particle number cuts.

Since the  $O_{M_{0,1,7}}$  and  $O_{T_{0,1,2}}$  operators are constrained tightly by  $WWjj$ ,  $WZjj$ , and  $ZZjj$  productions [61], we concentrate on the  $O_{M_{2,3,4,5}}$  and  $O_{T_{5,6,7}}$  operators.

##### 4.1 Implementation of unitarity bounds

To ensure that the events are generated by the EFT in a valid region, the unitarity bounds are applied as cuts on  $\hat{s}$ . However,  $\hat{s}$  is not an observable because of the invisible neutrino. Instead, we find an observable to evaluate  $\hat{s}$  approximately. We use the approximation that most of the  $W$  bosons are on shell, such that  $(p_{\ell} + p_{\nu})^2 \approx M_W^2 \ll \hat{s}$ . Compared with a large  $\hat{s}$ , the mass of the  $W$  boson is negligible; therefore,  $2p_{\ell}p_{\nu} \approx 0$ , which indicates that the flight direction of the neutrino is close to the charged lepton. We use an event selection strategy to select the events with a small azimuth angle between the charged lepton and the missing momentum, which is denoted as  $\Delta\phi_{\ell m}$ , to strengthen this approximation. The normalized distributions of  $\cos(\Delta\phi_{\ell m})$  are depicted in Fig. 3(a). The

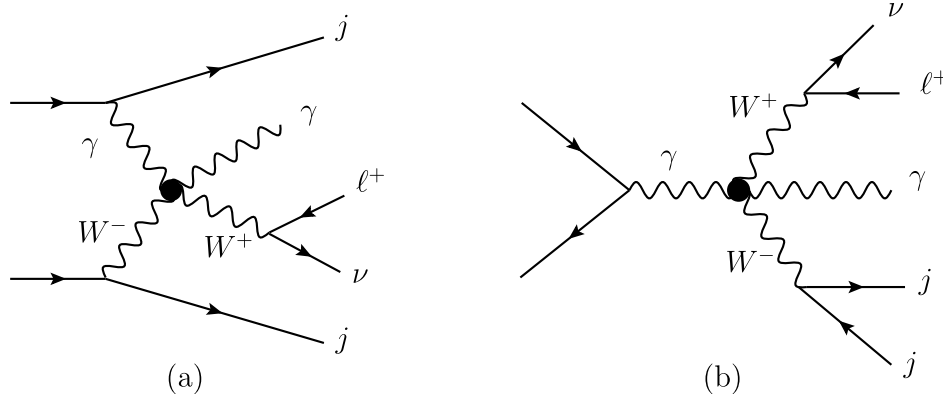


Fig. 1. Typical aQGC diagrams contributing to  $\ell^+ \nu \gamma jj$  final states. As in the SM, there are also VBS contributions as depicted in (a) and non-VBS contributions as in (b).

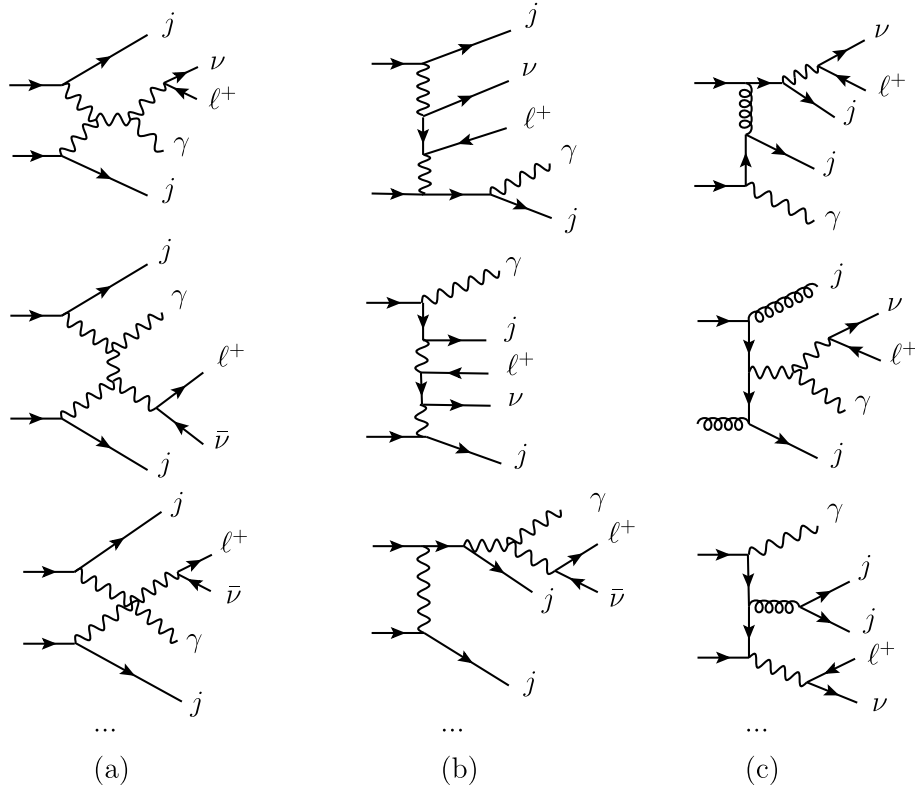


Fig. 2. Typical Feynman diagrams of SM backgrounds including (a) EW-VBS, (b) EW-non-VBS, and (c) QCD diagrams.

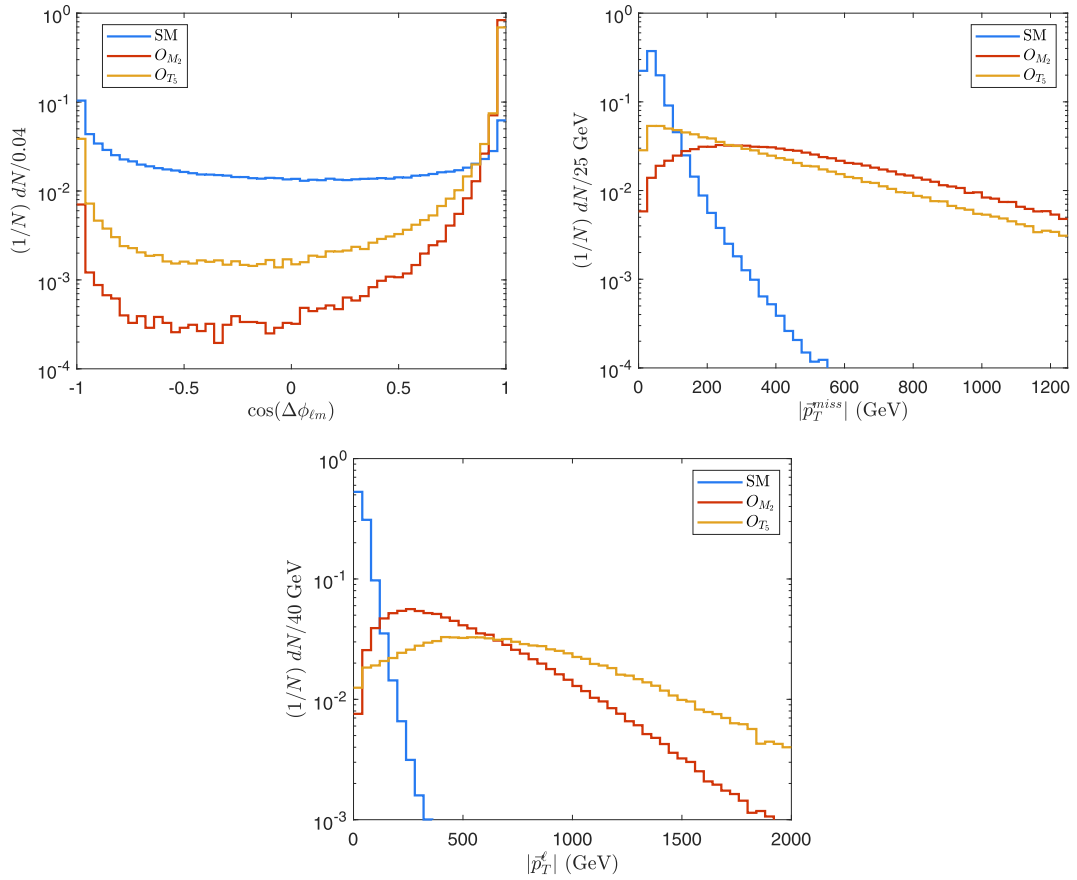


Fig. 3. (color online) Normalized distributions of  $\cos(\Delta\phi_{\ell m})$ ,  $|\vec{p}_T^{\text{miss}}|$ , and  $|\vec{p}_T^{\ell}|$  after particle number cuts.

distributions are similar for each class of operators (i.e.,  $O_{M_i}$  or  $O_{T_i}$ ), but are different between  $O_{M_i}$  and  $O_{T_i}$ . Therefore, we present only  $O_{M_2}$  and  $O_{T_5}$  as examples. We choose  $\cos(\Delta\phi_{\ell m}) > 0.95$  to cut off the events with a small  $\cos(\Delta\phi_{\ell m})$ .

Using the approximation that the neutrino and charged lepton are nearly parallel to each other, and by also requiring  $|\vec{p}_T^\ell| > 0$ , which is guaranteed due to the detector simulation, we introduce

$$\tilde{s} = \left( \sqrt{|\vec{p}_T^{\text{miss}}|^2 + \left( \frac{|\vec{p}_T^{\text{miss}}|}{|\vec{p}_T^\ell|} p_z^\ell \right)^2} + E_\ell + E_\gamma \right)^2 - \left( \left( 1 + \frac{|\vec{p}_T^{\text{miss}}|}{|\vec{p}_T^\ell|} \right) p_z^\ell + p_z^\gamma \right)^2 - |\vec{p}_T^\ell + \vec{p}_T^{\text{miss}} + \vec{p}_T^\gamma|^2, \quad (16)$$

where  $E_{\ell,\gamma} = \sqrt{(p_x^{\ell,\gamma})^2 + (p_y^{\ell,\gamma})^2 + (p_z^{\ell,\gamma})^2}$ ,  $\vec{p}_T^\ell = (p_x^\ell, p_y^\ell, 0)$ ,  $p_{x,y,z}^{\ell,\gamma}$  are components of the momenta of lepton and photon in the c.m. frame of  $pp$ , and  $\vec{p}_T^{\text{miss}}$  is the missing momentum.  $\tilde{s}$  reconstructs  $\hat{s}$  when the neutrino and charged lepton are exactly collinear and when the miss-

ing momentum is exactly neutrino transverse momentum. From the definition of  $\tilde{s}$ , one can see that, with a larger  $|\vec{p}_T^\ell|$ , the approximation is better. Meanwhile, the cross sections of the sub-processes  $W^+\gamma \rightarrow W^+\gamma$  and  $ZW^+ \rightarrow W^+\gamma$  increase with  $\sqrt{\hat{s}}$ . Therefore, one can expect that the number of signal events increases with increasing  $\hat{s}$ , namely, one can expect an energetic  $W^+$  boson. Therefore, the momentum of the charged lepton produced by the  $W^+$  boson should also be large. For the same reason,  $|\vec{p}_T^{\text{miss}}|$  should also be large. A small  $|\vec{p}_T^{\text{miss}}|$  probably indicates a neutrino along the  $\vec{z}$  direction. Approximation  $\tilde{s}$  can benefit from cutting off such events. The normalized distributions of  $|\vec{p}_T^\ell|$  and  $|\vec{p}_T^{\text{miss}}|$  after particle number cuts are shown in Fig. 3(b) and (c). We choose the events with  $|\vec{p}_T^\ell| > 80$  GeV and  $|\vec{p}_T^{\text{miss}}| > 50$  GeV.

To verify the approximation accuracy, we calculate both  $\hat{s}$  and  $\tilde{s}$ . Unlike real experiments, in simulation,  $\hat{s}$  can be obtained before detector simulation. Both  $\hat{s}$  and  $\tilde{s}$  are calculated after the  $\Delta\phi_{\ell m}$ ,  $|\vec{p}_T^\ell|$ , and  $|\vec{p}_T^{\text{miss}}|$  cuts are applied. Consider  $O_{M_2}$  and  $O_{T_5}$  operators for example, as shown in Fig. 4.  $\tilde{s}$  can approximate  $\hat{s}$  well.

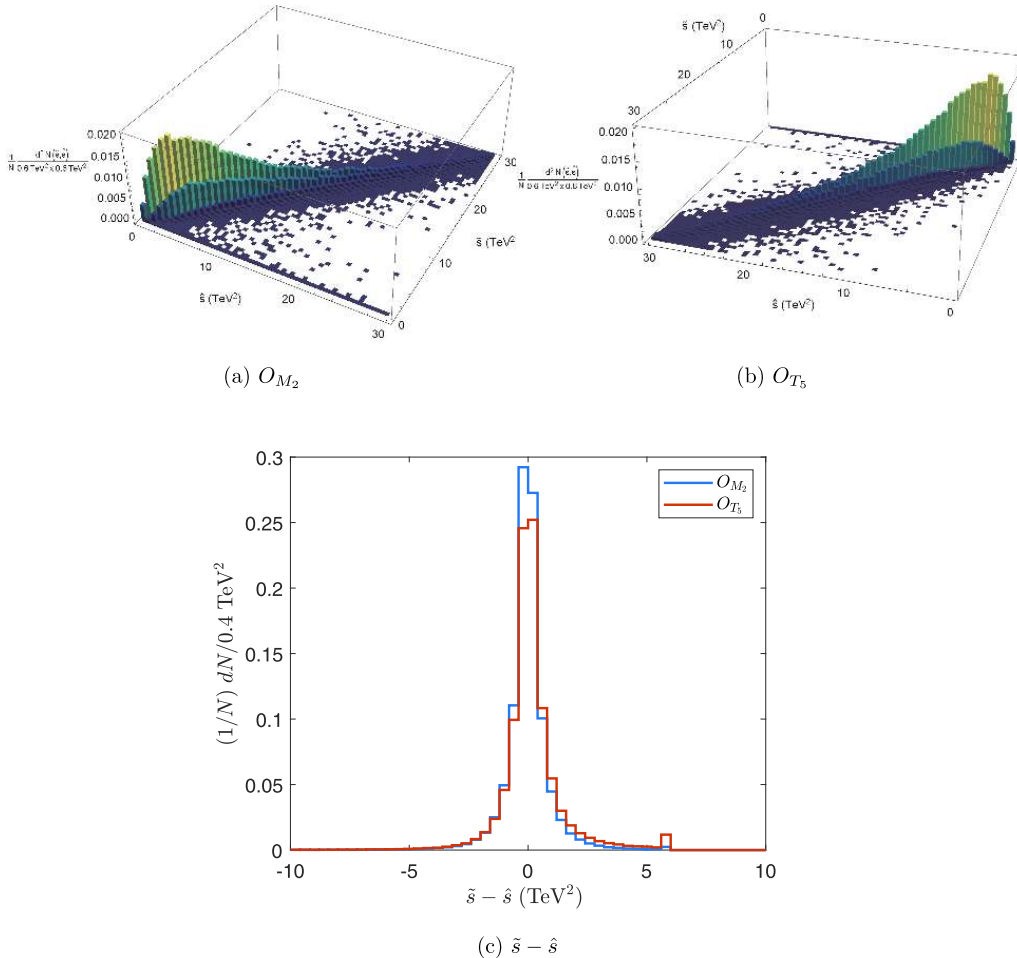


Fig. 4. (color online) Correlation between  $\hat{s}$  and  $\tilde{s}$  for  $O_{M_2}$  and  $O_{T_5}$ .

The unitarity bounds are realized as energy cuts using  $\tilde{s}$ , denoted as  $\tilde{s}_U$ . From Eq. (14), the  $\tilde{s}_U$  cuts are

$$\begin{aligned}\tilde{s}(f_{M_2}) &\leq \sqrt{\frac{s_W^2 256\pi M_W^2 \Lambda^4}{c_W^2 e^2 v^2 |f_{M_2}|}}, & \tilde{s}(f_{M_3}) &\leq \sqrt{\frac{384\pi s_W^2 M_W^2 \Lambda^4}{c_W^2 e^2 v^2 |f_{M_3}|}}, \\ \tilde{s}(f_{M_4}) &\leq \sqrt{\frac{512\pi M_W M_Z s_W^2 \Lambda^4}{e^2 v^2 |f_{M_4}|}}, & \tilde{s}(f_{M_5}) &\leq \sqrt{\frac{384\pi M_W M_Z s_W \Lambda^4}{c_W e^2 v^2 |f_{M_5}|}}, \\ \tilde{s}(f_{T_5}) &\leq \sqrt{\frac{40\pi \Lambda^4}{c_W^2 |f_{T_5}|}}, & \tilde{s}(f_{T_6}) &\leq \sqrt{\frac{32\pi \Lambda^4}{c_W^2 |f_{T_6}|}}, & \tilde{s}(f_{T_7}) &\leq \sqrt{\frac{64\pi \Lambda^4}{c_W^2 |f_{T_7}|}}.\end{aligned}\quad (17)$$

The effects of the  $\Delta\phi_{\ell m}$ ,  $|\vec{p}_T^\ell|$ ,  $|\vec{p}_T^{\text{miss}}|$ , and  $\tilde{s}_U$  cuts are shown in Table 4. Theoretically, the unitarity bounds should not be applied to the SM backgrounds. However, in the aspect of the experiment, we cannot distinguish the aQGC signals from the SM backgrounds strictly. Thus, the  $\tilde{s}_U$  cut can only be applied on all events. Therefore, we also apply the  $\tilde{s}_U$  cuts on the SM backgrounds. We verify that the  $\tilde{s}_U$  cuts have negligible effects on the SM backgrounds for all the largest  $f_{M_{2,3,4,5}}/\Lambda^4$  and  $f_{T_{5,6,7}}/\Lambda^4$  we are using.

From Table 4, it is evident that the unitarity bounds have significant suppressive impacts on the signals, particularly for the  $O_{M_i}$  operators, indicating the necessity of the unitarity bounds.

## 4.2 Kinematic features of aQGCs

As already mentioned, the VBS processes do not increase with  $\sqrt{\hat{s}}$  in the SM. This opens a window to detect aQGCs. To focus on the VBS contributions, we investigate the efficiencies of the standard VBS/VBF cuts [21]. The VBS/VBF cuts are designed to highlight the VBS contributions from the SM and BSM; however, they cannot cut off the SM VBS contributions. Therefore, they are not as efficient as other cuts designed for aQGCs only. We impose only  $|\Delta y_{jj}|$ , which is defined as the difference between the pseudo rapidities of the two hardest jets. The normalized distributions of  $|\Delta y_{jj}|$  are depicted in Fig.

5(a). It is evident that  $|\Delta y_{jj}|$  is an efficient cut for the  $O_{M_i}$  operators, and we select the events with  $|\Delta y_{jj}| > 1.5$ .

For the lepton and photon, the cuts are mainly to select events with large  $\hat{s}$ . The normalized distributions of  $\hat{s}$  are shown in Fig. 5(b). We select the events with  $\hat{s} > 0.4$  TeV<sup>2</sup>. To distinguish from the  $\tilde{s}_U$  cut,  $\tilde{s}$  cut in this subsection is denoted as  $\tilde{s}^{\text{cut}}$ .

There are other sensitive observables to select large  $\hat{s}$  events, such as the invariant mass of the charged lepton and photon defined as  $M_{\ell\gamma} = \sqrt{(p_\ell + p_\gamma)^2}$ , and the angle between the photon and charged lepton. We find that, after the  $\tilde{s}^{\text{cut}}$  cut, the other cuts are redundant. Consider  $M_{\ell\gamma}$  as an example. The normalized distributions of  $M_{\ell\gamma}$  are shown in Fig. 5(c). As shown,  $M_{\ell\gamma}$  is a significantly sensitive observable, and  $M_{\ell\gamma} > M_{\ell\gamma}^{\text{cut}}$  can be used as an efficient cut. However, note that after  $\tilde{s}^{\text{cut}}$ , due to  $M_{\ell\gamma} \leq \sqrt{\hat{s}}$ , one must choose a significantly large  $M_{\ell\gamma}^{\text{cut}}$ , which is almost equivalent to a large  $\tilde{s}^{\text{cut}}$ .

## 4.3 Polarization features of aQGCs

To improve the event select strategy, we investigate the polarization features that are less correlated with  $\tilde{s}$ . As is evident from Tables 2 and 3, for  $O_{M_i}$ , the leading contributions of the signals are those with longitudinal  $W^+$  bosons in the final states, whereas for  $O_{T_i}$ , both the left- and right-handed  $W^+$  bosons dominate. The polarization of the  $W^+$  boson can be inferred by the momentum of the charged lepton in the  $W^+$  boson rest-frame, the so called helicity frame, as [76]

$$\frac{d\sigma}{d\cos\theta^*} \propto f_L \frac{(1 - \cos(\theta^*))^2}{4} + f_R \frac{(1 + \cos(\theta^*))^2}{4} + f_0 \frac{\sin^2(\theta^*)}{2}, \quad (18)$$

where  $\theta^*$  is the angle between the flight directions of  $\ell^+$  and  $W^+$  in the helicity frame;  $f_L$ ,  $f_R$ , and  $f_0 = 1 - f_L - f_R$  are the fractions of the left-handed, right-handed, and longitudinal polarizations, respectively. Because the neutrinos are invisible, it is difficult to reconstruct the momentum of the  $W^+$  boson and boost the lepton to the rest

Table 4. Cross sections of SM backgrounds and signals for various operators after  $N_{j\gamma,\ell^+}$ ,  $\Delta\phi_{\ell m}$ ,  $|\vec{p}_T^\ell|$ ,  $|\vec{p}_T^{\text{miss}}|$ , and  $\tilde{s}_U$  cuts. The maximum  $\tilde{s}$  used in the  $\tilde{s}_U$  cuts are obtained using the upper bounds of  $f_X/\Lambda^4$  in Table 1 and Eq. (17).

Channel/fb	no cut	$N_{j\gamma,\ell^+}$	$\Delta\phi_{\ell m}$	$ \vec{p}_T^\ell $	$ \vec{p}_T^{\text{miss}} $	$\tilde{s}_U$
SM	9520.8	3016.6	211.7	65.1	40.6	–
$O_{M_2}$	6.353	4.06	3.51	3.45	3.43	0.93
$O_{M_3}$	21.05	13.62	12.13	11.95	11.90	2.19
$O_{M_4}$	7.39	4.81	4.06	3.94	3.92	1.03
$O_{M_5}$	25.23	16.73	14.75	14.49	14.42	4.05
$O_{T_5}$	2.71	1.77	1.28	1.25	1.22	0.72
$O_{T_6}$	16.92	11.19	8.94	8.36	8.26	3.06
$O_{T_7}$	7.47	4.97	3.97	3.69	3.65	1.43

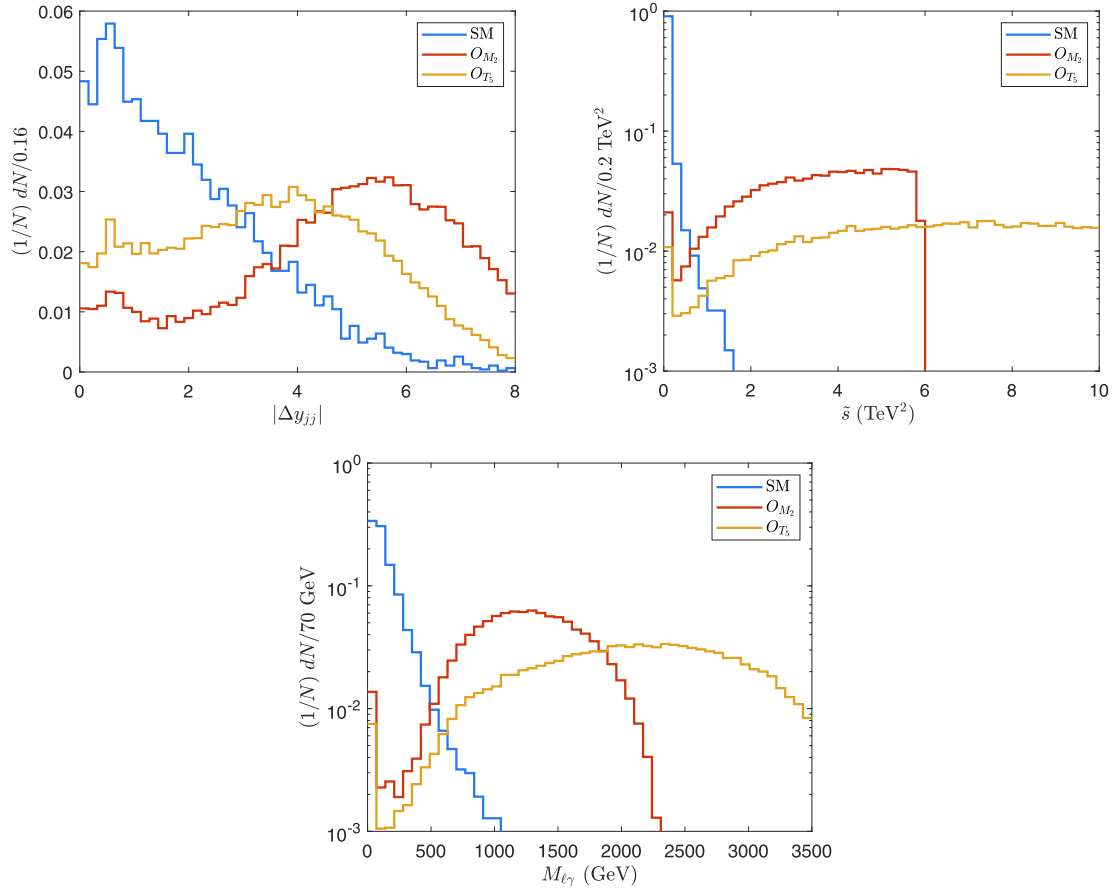


Fig. 5. (color online) Normalized distributions of  $|\Delta y_{jj}|$ ,  $\bar{s}$ , and  $M_{\ell\gamma}$  after  $\bar{s}_U$  cut.

frame of the  $W^+$  boson. However, when the transverse momentum of the  $W^+$  boson is large,  $\cos(\theta^*)$  can be obtained approximately as  $\cos(\theta^*) \approx 2(L_p - 1)$  with  $L_p$  defined as [58]

$$L_p = \frac{\vec{p}_T^\ell \cdot \vec{p}_T^W}{|\vec{p}_T^W|^2}, \quad (19)$$

where  $\vec{p}_T^W = \vec{p}_T^\ell + \vec{p}_T^{\text{miss}}$ . For the signal events of the  $O_{M_i}$  or  $O_{T_i}$  operators, the polarization fractions of the  $W^+$  bosons are different from those in the SM backgrounds. The polarization fractions can be categorized into four patterns: the SM,  $O_{M_i}$ ,  $O_{T_{0.5}}$ , and  $O_{T_{1,2,6,7}}$  patterns.  $O_{M_2}$ ,  $O_{T_5}$ , and  $O_{T_7}$  are chosen as the representations. Neglecting the events with  $L_p \notin [0, 1]$ , the normalized distributions of  $L_p$  after  $\bar{s}_U$  cuts are depicted in Fig. 6.

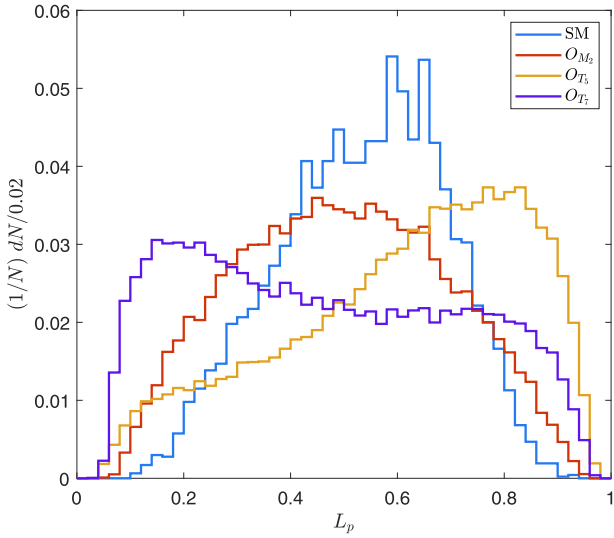
As presented in Tables 2 and 3, the polarization of the  $W^+$  boson is related to  $\theta$ , which is the angle between the outgoing photon and the  $\vec{z}$ -axis of the c.m. frame of the sub-process; however,  $\theta$  is not an observable. Because the protons are energetic, we assume that the vector bosons in the initial states of the sub-processes carry large fractions of proton momenta. Therefore, their flight directions are close to the protons in the c.m. frame. In this way,  $\theta$  could be approximately estimated using the angle

between outgoing photons and the  $\vec{z}$ -axis of the c.m. frame of protons, which is denoted as  $\theta'$ . The correlation features between  $\theta'$  and  $L_p$  can be used to extract the aQGC signal events from the SM backgrounds. The correlations of  $\theta'$  and  $L_p$  for the SM, and for the  $O_{M_2}$ ,  $O_{T_5}$ , and  $O_{T_7}$  operators are established in Fig. 7. From Fig. 7, it is evident that signal events of  $O_{T_{5,7}}$  distribute differently from the SM backgrounds. The distribution for the SM peaks at  $|\cos(\theta')| \approx 1$  and  $L_p \approx 0.5$ , the distribution for  $O_{T_5}$  peaks at  $|\cos(\theta')| \approx 1$  and  $L_p \approx 0$ , and the distribution for  $O_{T_7}$  peaks at  $|\cos(\theta')| \approx 1$  and  $L_p \approx 1$ . Therefore, we define

$$r = (1 - |\cos(\theta')|)^2 + \left(\frac{1}{2} - L_p\right)^2, \quad (20)$$

where  $r$  is a sensitive observable that can be used as a cut to discriminate the signals of the  $O_{T_{5,6,7}}$  operators from the SM backgrounds. The normalized distributions are shown in Fig. 8. We select the events with  $r > 0.05$ .

To verify that  $r$  cut is not redundant, we calculate the correlation between  $\bar{s}$  and  $M_{\ell\gamma}$ , and compare it with the correlation between  $\bar{s}$  and  $r$ . Consider the SM backgrounds and the signal of  $O_{T_5}$  as examples. The results are shown in Fig. 9. It is evident that the events with small  $M_{\ell\gamma}$  are almost those with small  $\bar{s}$ ; however, the


 Fig. 6. (color online) Normalized distributions of  $L_p$ .

same is not the case for  $r$ .

#### 4.4 Summary of cuts

For various operators, the kinematic and polarization features are different. Therefore, we propose to use various cuts to search for different operators, as summarized

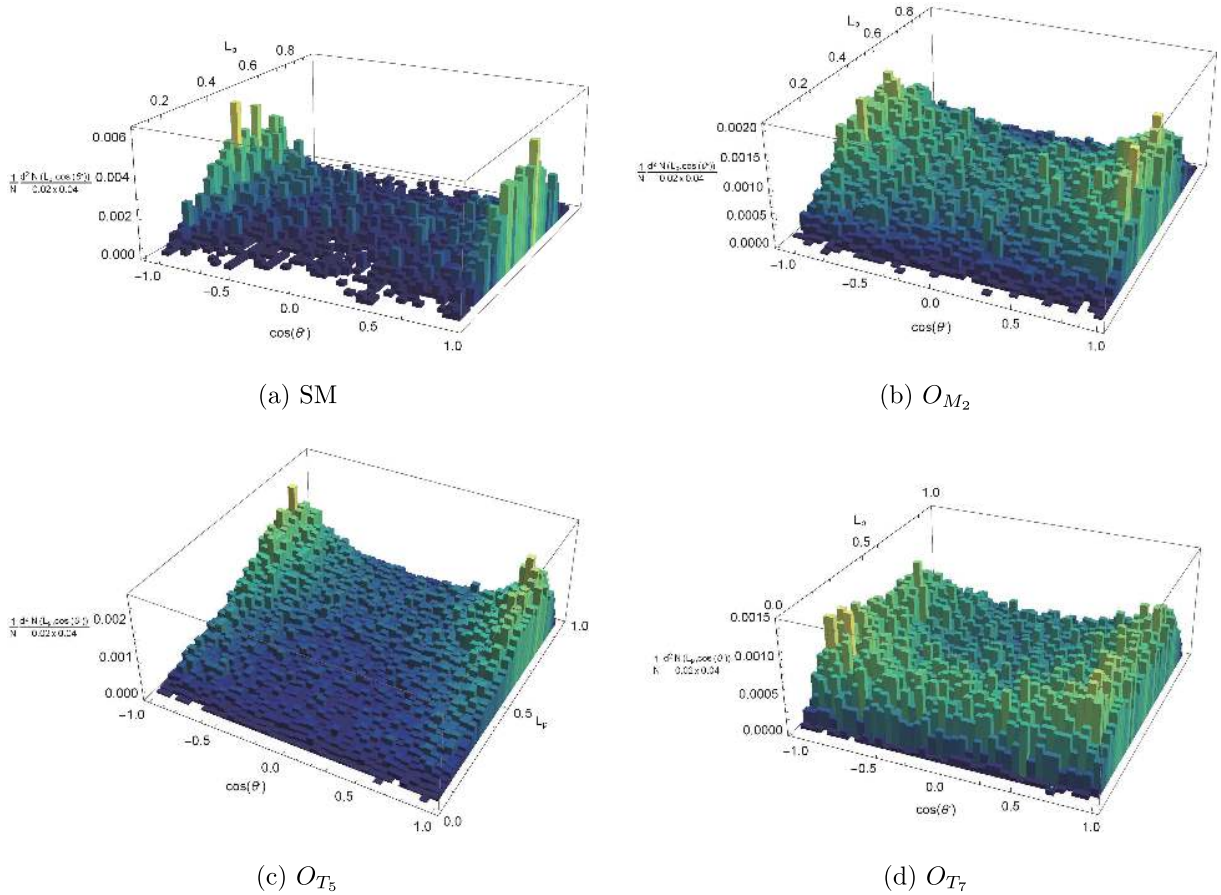
in Table 5. Note that  $\tilde{s}^{\text{cut}}$  in fact also cut off all the events with small  $M_{\ell\gamma}$ . Therefore,  $|M_{\ell\gamma} - M_Z| > 10 \text{ GeV}$  is satisfied. The latter is used to reduce the backgrounds from  $Z \rightarrow \ell\ell$  with one  $\ell$  mis-tagged as a photon in the previous study of  $W\gamma jj$  production [39], and  $\tilde{s}^{\text{cut}}$  has a similar effect.

The results are shown in Table 6. The statistical error is negligible compared with the systematic error; therefore, it is not presented. The large SM backgrounds can be reduced effectively using our selection strategy.

## 5 Cross sections and statistical significances

To investigate the signals of aQGCs, one should investigate how the cross section is modified by adding dimension-8 operators to the SM Lagrangian. Furthermore, the effect of interference is also included. In this section, we investigate the process  $pp \rightarrow \ell^+ \nu \gamma jj$  with all Feynman diagrams including non-VBS aQGC diagrams, such as Fig. 1(b), and with all possible interference effects.

To investigate the parameter space, we generate events with each operator individually. The unitarity bounds are set as  $\tilde{s}_U$  cuts, which depend on  $f_{M_i}/\Lambda^4$  and


 Fig. 7. (color online) Normalized distributions of  $L_p$  and  $\cos\theta$ . Each bin corresponds to  $dL_p \times d(\cos\theta) = 0.02 \times 0.04$  ( $50 \times 50$  bins).

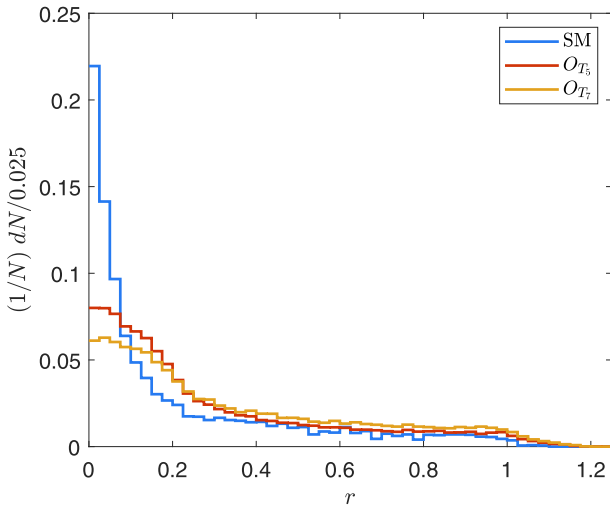
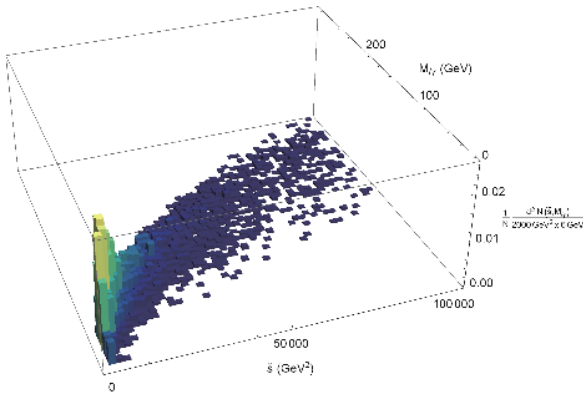


Fig. 8. (color online) Normalized distributions of  $r$  after  $\tilde{s}_U$  cut.

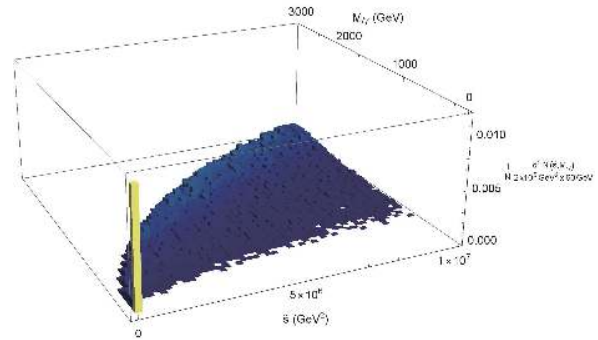
$f_{T_i}/\Lambda^4$  used to generate the events. The cross sections as

functions of  $f_{M_i}/\Lambda^4$  and  $f_{T_i}/\Lambda^4$  are shown in Figs. 10 and 11. The results with and without the unitarity bounds are presented. As is evident from Figs. 10 and 11, the cross sections are approximately bilinear functions of  $f_{M_i}/\Lambda^4$  and  $f_{T_i}/\Lambda^4$  without the unitarity bounds. However, the unitarity bounds significantly suppress the signals, and the resulting cross sections are no longer bilinear functions. From Figs. 10 and 11, it is also evident that the  $W\gamma jj$  production is more sensitive to the  $O_{M_{3,5}}$  and  $O_{T_{6,7}}$  operators.

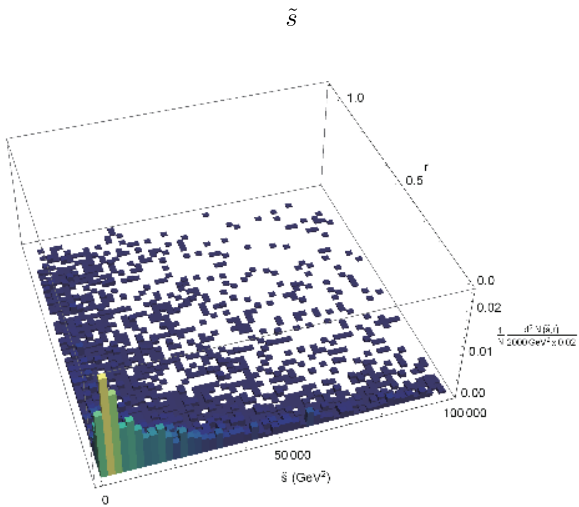
The constraints on operator coefficients can be estimated with the help of statistical significance defined as  $S_{\text{stat}} \equiv N_S / \sqrt{N_S + N_B}$ , where  $N_S$  is the number of signal events and  $N_B$  is the number of the background events. The total luminosity,  $\mathcal{L}$ , at 13 TeV for the years 2016, 2017, and 2018 is  $\mathcal{L} \approx 137.1 \text{ fb}^{-1}$  [77]. For each  $f_X/\Lambda^4$  used to generate the events, the  $\tilde{s}_U$  cut can be set accordingly; subsequently,  $S_{\text{stat}}$  at  $137.1 \text{ fb}^{-1}$  and 13 TeV can be obtained. The constraints are set by the lowest positive  $f_X/\Lambda^4$  and the greatest negative  $f_X/\Lambda^4$  with  $S_{\text{stat}}$  larger



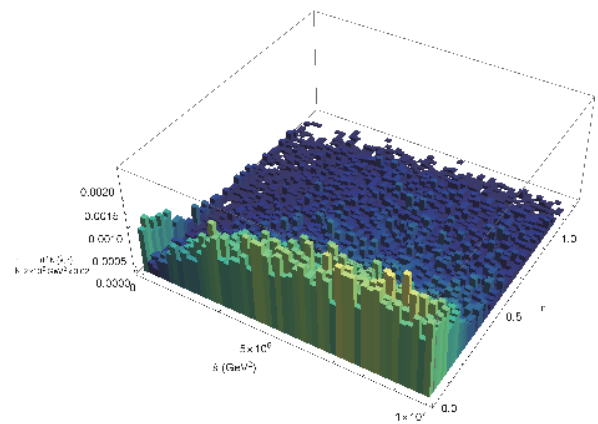
(a) SM backgrounds, correlation between  $M_{\ell\gamma}$  and



(b)  $O_{T_5}$ , correlation between  $M_{\ell\gamma}$  and  $\tilde{s}$



(c) SM backgrounds, correlation between  $r$  and  $\tilde{s}$



(d)  $O_{T_5}$ , correlation between  $r$  and  $\tilde{s}$

Fig. 9. (color online) Correlations between  $M_{\ell\gamma}$  and  $\tilde{s}$  (upper panels),  $r$  and  $\tilde{s}$  (bottom panels) for  $O_{T_5}$ , and the SM backgrounds.

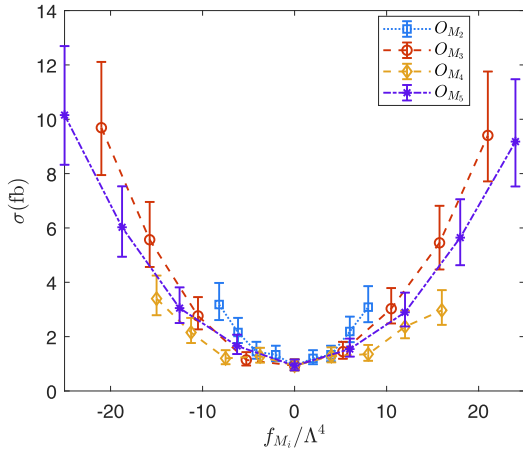
Table 5. Two classes of cuts.

$O_{M_i}$	$O_{T_{5,6,7}}$
$\tilde{s} > 0.4 \text{ TeV}^2$	$\tilde{s} > 0.4 \text{ TeV}^2$
$ \Delta y_{jj}  > 1.5$	$0 \leq L_p \leq 1, r > 0.05$

than the required statistical significance. The constraints on the coefficients at current luminosity are depicted in Table 7. Comparing the constraints from 13 TeV CMS experiments in Table 1 with the ones in Table 7, it is evident that, even with the unitarity bounds suppressing the signals, the allowed parameter space can still be reduced significantly using our efficient event selection strategy.

## 6 Summary

The accurate measurement of VBS processes at the

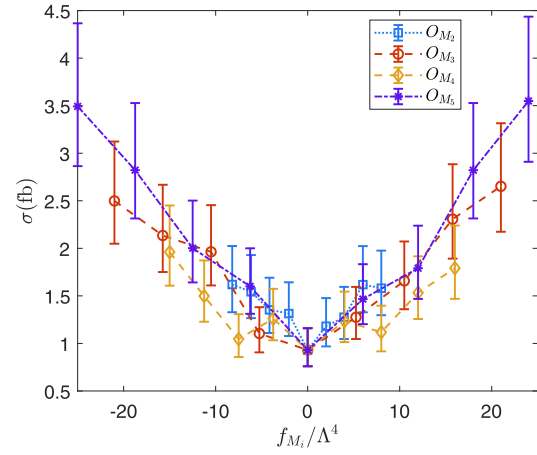


(a) without unitarity bounds

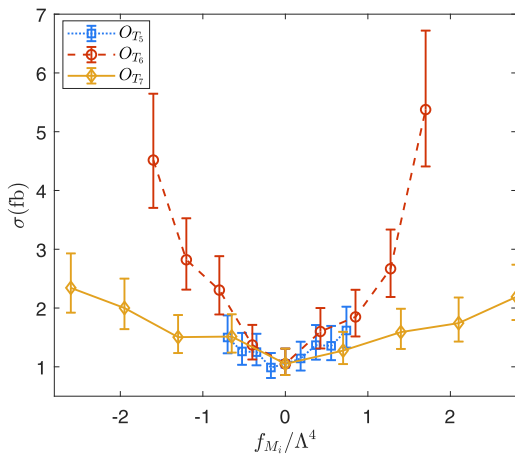
 Table 6. Cross sections (fb) of signals and SM backgrounds after  $\tilde{s}^{\text{cut}}$ ,  $|\Delta y_{jj}|$ , and  $r$  cuts. The column "After  $\tilde{s}_U$ " is the same as the last column in Table 4.

Channel	after $\tilde{s}_U$	after $\tilde{s}^{\text{cut}}$	$ \Delta y_{jj} $ or $r$
SM	40.6	1.70	$0.93^{+0.23}_{-0.17}$ ( $\Delta y_{jj}$ )
			$1.05^{+0.26}_{-0.19}$ ( $r$ )
$O_{M_2}$	0.93	0.91	$0.82^{+0.20}_{-0.15}$
$O_{M_3}$	2.19	2.11	$1.90^{+0.48}_{-0.35}$
$O_{M_4}$	1.03	1.01	$0.91^{+0.23}_{-0.16}$
$O_{M_5}$	4.05	3.94	$3.55^{+0.89}_{-0.64}$
$O_{T_5}$	0.72	0.71	$0.60^{+0.15}_{-0.11}$
$O_{T_6}$	3.06	3.01	$2.69^{+0.62}_{-0.48}$
$O_{T_7}$	1.43	1.40	$1.12^{+0.28}_{-0.20}$

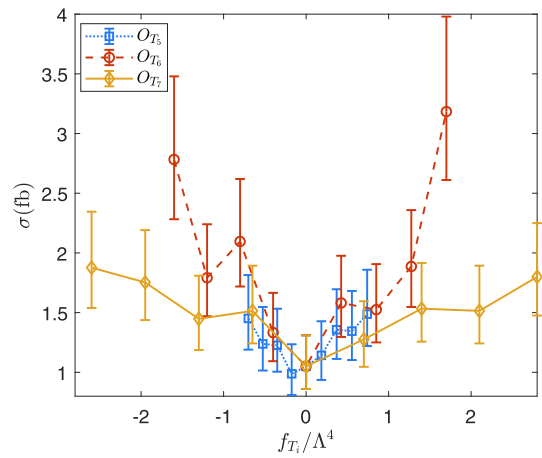
LHC is very important for the understanding of the SM and search of BSM. In recent years, the VBS processes



(b) with unitarity bounds

 Fig. 10. (color online) Cross sections as functions of  $f_{M_i}/\Lambda^4$  with and without unitarity bounds.


(a) without unitarity bounds



(b) with unitarity bounds

 Fig. 11. (color online) Cross sections as functions of  $f_{T_{i,j}}/\Lambda^4$  with and without unitarity bounds.

Table 7. Constraints on operators at LHC with  $\mathcal{L} = 137.1 \text{ fb}^{-1}$ .

Coefficients	$\mathcal{S}_{\text{stat}} > 2$	Coefficients	$\mathcal{S}_{\text{stat}} > 2$
$f_{M_2}/\Lambda^4$	[-2.05, 2.0]	$fr_3/\Lambda^4$	[-0.525, 0.37]
$f_{M_3}/\Lambda^4$	[-10.5, 5.25]	$fr_6/\Lambda^4$	[-0.4, 0.425]
$f_{M_4}/\Lambda^4$	[-11.25, 4.0]	$fr_7/\Lambda^4$	[-0.65, 0.7]
$f_{M_5}/\Lambda^4$	[-6.25, 6.0]		

have received significant attention and been studied extensively. To investigate the signals of BSM, a model independent approach, known as the SMEFT, is used frequently. The effects of BSM show up as higher dimensional operators. The VBS processes can be used to probe dimension-8 anomalous quartic gauge-boson operators. In this study, we focused on the effects of aQGCs in the  $pp \rightarrow W\gamma jj$  process. The operators concerned are summarized, and the corresponding vertices are obtained.

An important consideration regarding the SMEFT is that of its validity. We studied the validity of the SMEFT using the partial-wave unitarity bound, which sets an upper bound on  $\hat{s}^2|f_X|$ , where  $f_X$  is the coefficient of operator  $O_X$ . In other words, there exists a maximum  $\hat{s}$  for a fixed coefficient in the sense of unitarity. We discard all the events with  $\hat{s}$  larger than the maximally allowed one, so that the results obtained via the SMEFT are guaranteed to respect unitarity. For this purpose, we find an ob-

servable that can approximate  $\hat{s}$  very well, denoted as  $\tilde{s}$ , based on which the unitarity bounds are applied. Due to the fact that there are massive  $W^+$  or/and  $Z$  bosons in the initial state of the sub-process, and that the massive particle emitting from a proton can carry a large fraction of the proton momentum, the c.m. energy of the sub-process is found to be of the same order as the c.m. energy of the corresponding process. As a consequence, at large c.m. energy, the unitarity bounds are very strict, and the cuts can significantly reduce the signals.

To study the discovery potential of aQGCs, we investigate the kinematic features of the signals induced by aQGCs and find that  $\tilde{s}$  serves as a very efficient cut to highlight the signals. We also find that other cuts to cut off the events with small  $\hat{s}$  are redundant. To find other sensitive observables less correlated with  $\hat{s}$ , we investigate the polarization features of the signals. The polarization features of  $O_{T_i}$  operators are found to be very different from the SM backgrounds. We find a sensitive observable  $r$  to select the signal events of the  $O_{T_i}$  operators. Although the signals of aQGCs are highly suppressed by unitarity bounds, the constraints on the coefficients for the  $O_{M_{2,3,4,5}}$  and  $O_{T_{5,6,7}}$  operators can still be tightened significantly with current luminosity at 13 TeV LHC.

*We thank Jian Wang and Cen Zhang for useful discussions.*

## References

- B. W. Lee, C. Quigg, and H. B. Thacker, *Phys. Rev. D*, **16**: 1519 (1977)
- C. Zhang and S.-Y. Zhou, *Phys. Rev. D*, **100**: 095003 (2019)
- Q. Bi, C. Zhang, and S.-Y. Zhou, *JHEP*, **06**: 137 (2019)
- B. Grzadkowski *et al.*, *JHEP*, **10**: 085 (2010)
- S. Willenbrock and C. Zhang, *Ann. Rev. Nucl. Part. Sci.*, **64**: 83-100 (2014)
- E. Massó, *JHEP*, **10**: 128 (2014)
- M. Maniatis, A. von Manteuffel, and O. Nachtmann, *Nucl. Phys. B Proc. Suppl.*, **179-180**: 104-108 (2008)
- R. L. Delgado, A. Dobado, M. J. Herrero *et al.*, *JHEP*, **07**: 149 (2014)
- D. Espriu and F. Mescia, *Phys. Rev. D*, **90**: 015035 (2014)
- S. Fichtel and G. von Gersdorff, *JHEP*, **03**: 102 (2014)
- T. D. Lee, *Phys. Rev. D*, **8**: 1226 (1973)
- G. C. Branco, P. M. Ferreira, L. Lavoura *et al.*, *Phys. Rep.*, **516**: 1 (2012)
- I. F. Ginzburg and M. Krawczyk, *Phys. Rev. D*, **72**: 115013 (2005)
- J.-C. Yang and M.-Z. Yang, *Mod. Phys. Lett. A*, **31**: 1650012 (2016)
- X.-G. He, G. C. Joshi, H. Lew *et al.*, *Phys. Rev. D*, **44**: 2118 (1991)
- J.-X. Hou and C.-X. Yue, *Eur. Phys. J. C*, **79**: 938 (2019)
- K. Mimasu and V. Sanz, arXiv: 1409.4792[hep-ph]
- C.-X. Yue, M.-Z. Liu, and Y.-C. Guo, *Phys. Rev. D*, **100**: 015020 (2019)
- D. R. Green, P. Meade, and M. A. Pleier, *Rev. Mod. Phys.*, **89**: 035008 (2017)
- S. Brass, C. Fleper, W. Kilian *et al.*, *Eur. Phys. J. C*, **78**: 931 (2018)
- M. Rauch, arXiv: 1610.08420[hep-ph]
- C. F. Anders *et al.*, *Rev. Phys.*, **3**: 44-63 (2018)
- J. Chang *et al.*, *Phys. Rev. D*, **87**: 093005 (2013)
- J. Ellis, S.-F. Ge, H.-J. He *et al.*, *Chin. Phys. C*, **44**: 063106 (2020)
- M. Born and L. Infeld, *Proc. R. Soc. Lond. A*, **144**: 425-451 (1934)
- E. S. Fradkin and A. A. Tseytlin, *Phys. Lett. B*, **163**: 123-130 (1985)
- C. Bachas, *Phys. Lett. B*, **374**: 37-42 (1996)
- J. Ellis and S.-F. Ge, *Phys. Rev. Lett.*, **121**: 041801 (2018)
- M. S. Chanowitz and M. K. Gaillard, *Nucl. Phys. B*, **261**: 379-431 (1985)
- G. Aad *et al.* (ATLAS Collaboration), *Phys. Rev. Lett.*, **113**: 141803 (2014)
- V. Khachatryan *et al.* (C. M. S. Collaboration), *Phys. Rev. Lett.*, **114**: 051801 (2015)
- V. Khachatryan *et al.* (C. M. S. Collaboration), *Phys. Lett. B*, **770**: 380-402 (2017)
- M. Aaboud *et al.* (ATLAS collaboration), *JHEP*, **07**: 107 (2017)
- A. M. Sirunyan *et al.* (C. M. S. Collaboration), *Phys. Lett. B*, **774**: 682-705 (2017)
- A. M. Sirunyan *et al.* (C. M. S. Collaboration), *Phys. Lett. B*, **789**: 19-44 (2019)
- M. Aaboud *et al.* (ATLAS Collaboration), *Phys. Lett. B*, **793**: 469-492 (2019)
- A. M. Sirunyan *et al.* (C. M. S. Collaboration), *Phys. Lett. B*, **795**: 281-307 (2019)
- A. M. Sirunyan *et al.* (C. M. S. Collaboration), *Phys. Rev. Lett.*,

- 120**: 081801 (2018)
- 39 V. Khachatryan *et al.* (C. M. S. Collaboration), *JHEP*, **06**: 106 (2017)
- 40 Rafael L. Delgado, Antonio Dobado, Miguel Espada *et al.*, *JHEP*, **1811**: 010 (2018)
- 41 R. L. Delgado, A. Dobado, and F.J. Llanes-Estrada, *Eur. Phys. J. C*, **77**: 205 (2017)
- 42 V. Ari, E. Gurkanli, A. A. Billur *et al.*, arXiv: 1812.07187 [hep-ph]
- 43 V. Ari, E. Gurkanli, A. Gutiérrez-Rodríguez *et al.*, *Eur. Phys. J. Plus* **135**: 336(2020)
- 44 Y.-C. Guo, Y.-Y. Wang, and J.-C. Yang, arXiv: 1912.10686[hep-ph]
- 45 F. Campanario, N. Kaiser, and D. Zeppenfeld, *Phys. Rev. D*, **89**: 014009 (2014)
- 46 T. D. Lee and C. N. Yang, *Phys. Rev. Lett.*, **4**: 307 (1960)
- 47 M. Froissart, *Phys. Rev.*, **123**: 1053 (1961)
- 48 G. Passarino, *Nucl. Phys. B*, **343**: 31-59 (1990)
- 49 Roberto Contino *et al.*, *JHEP*, **07**: 144 (2016)
- 50 A. Ballestrero, E. Maina, and G. Pelliccioli, *JHEP*, **03**: 170 (2018)
- 51 R. Aaij *et al.* (LHCb collaboration), *JHEP*, **02**: 104 (2016)
- 52 S. D. Genon, L. Hofer, J. Matias *et al.*, *JHEP*, **06**: 092 (2016)
- 53 Z. Bern *et al.*, *Phys. Rev. D*, **84**: 034008 (2011)
- 54 W. J. Stirling and E. Vryonidou, *JHEP*, **07**: 124 (2012)
- 55 G. Aad *et al.* (ATLAS Collaboration), *Eur. Phys. J. C*, **72**: 2001 (2012)
- 56 V. Khachatryan *et al.* (C. M. S. Collaboration), *Phys. Lett. B*, **762**: 512-534 (2016)
- 57 M. Aaboud *et al.* (ATLAS Collaboration), *Eur. Phys. J. C*, **77**: 264 (2017)
- 58 S. Chatrchyan *et al.* (C. M. S. Collaboration), *Phys. Rev. Lett.*, **107**: 021802 (2011)
- 59 O. J. P. Éboli, M. C. Gonzalez-Garcia, and J. K. Mizukoshi, *Phys. Rev. D*, **74**: 073005 (2006)
- 60 O. J. P. Éboli and M. C. Gonzalez-Garcia, *Phys. Rev. D*, **93**: 093013 (2016)
- 61 A. M. Sirunyan *et al.* (C. M. S. Collaboration), *Phys. Lett. B*, **798**: 134985 (2019)
- 62 A. M. Sirunyan *et al.* (C. M. S. Collaboration), *JHEP*, **06**: 076 (2020)
- 63 M. Jacob and G. C. Wick, *Annals Phys.*, **7**: 404-428 (1959)
- 64 T. Corbett, O. J. P. Éboli, and M. C. Gonzalez-Garcia, *Phys. Rev. D*, **91**: 035014 (2014)
- 65 J. Layssac, F. M. Renard, and G. Gounaris, *Phys. Lett. B*, **332**: 146-152 (1994)
- 66 T. Corbett, O. J. P. Éboli, and M. C. Gonzalez-Garcia, *Phys. Rev. D*, **96**: 035006 (2017)
- 67 R. G. Ambrosio, *Acta Phys. Pol. B Proc. Suppl.*, **11**: 239 (2018)
- 68 G. Perez, M. Sekulla, and D. Zeppenfeld, *Eur. Phys. J. C*, **78**: 759 (2018)
- 69 W. Kilian, M. Sekulla, T. Ohl *et al.*, *Phys. Rev. D*, **91**: 096007 (2015)
- 70 C. Garcia-Garcia, M. J. Herrero, and R. A. Morales, *Phys. Rev. D*, **100**: 096003 (2019)
- 71 J. A. Aguilar Saavedra *et al.*, arXiv: 1802.07237[hep-ph]
- 72 J. Alwall *et al.*, *JHEP*, **1407**: 079 (2014)
- 73 R.D. Ball *et al.* (NNPDF collaboration), *Nucl. Phys. B*, **877**: 290 (2013)
- 74 T. Sjöstrand *et al.*, *Comput. Phys. Commun.*, **191**: 159 (2015)
- 75 J. de Favereau *et al.*, *J. High Energy Phys.*, **1402**: 057 (2014)
- 76 Marco Peruzzi, CERN preprint, CERN-THESIS-2011-088
- 77 A. M. Sirunyan *et al.* (C. M. S. Collaboration), *JHEP*, **03**: 051 (2020)